MATHEMATICAL SIMULATION OF LIGHT PULSE PROPAGATING WITHIN A MICRORING RESONATOR SYSTEM

BUDDHAPORN VANISHKORN

A THESIS SUBMITTED IN FULFILLMENT OF THE REQUIREMENT FOR THE DEGREE OF DOCTOR OF PHILOSOPHY IN APPLIED MATHEMATICS

DEPARTMENT OF MATHEMATICS
FACULTY OF SCIENCE
KING MONGKUT'S INSTITUTE OF TECHNOLOGY LADKRABANG

2015
KMITL-2015-SC-D-001-050

MATHEMATICAL SIMULATION OF LIGHT PULSE PROPAGATING WITHIN A MICRORING RESONATOR SYSTEM

BUDDHAPORN VANISHKORN

A THESIS SUBMITTED IN FULFILLMENT OF THE REQUIREMENT FOR THE DEGREE OF DOCTOR OF PHILOSOPHY IN APPLIED MATHEMATICS

DEPARTMENT OF MATHEMATICS
FACULTY OF SCIENCE
KING MONGKUT'S INSTITUTE OF TECHNOLOGY LADKRABANG

2015
KMITL-2015-SC-D-001-050

หัวข้อวิทยานิพนธ์	การจำลองเชิงคณิตศาสตร์ของการเคลื่อนที่ของพัลส์แสงภายในระบบโพรงสั่นพ้องวงแหวนขนาดเล็ก
ชื่อนักศึกษา	นาย พุทธพร วานิชกร
รหัสประจำตัว	52650202
ปริญญา	ปรัชญาดุษฎีบัณฑิต(คณิตศาสตร์ประยุกต์)
ภาควิชา	คณิตศาสตร์
พ.ศ.	2558
อาจารย์ที่ปรึกษาวิทยานิพนธ์	รองศาสตราจารย์ ดร. พันธนี พงศ์สัมพันธ์ (ปฏิบัติหน้าที่แทนอาจารย์ที่ปรึกษาวิทยานิพนธ์หลัก)

บทคัดย่อ

ในวิทยานิพนธ์นี้ใช้การจำลองเชิงคณิตศาสตร์เพื่อศึกษาผลที่ได้จากการเคลื่อนที่ของพัลส์แสงภายในระบบโพรงสั่นพ้องวงแหวน โดยมีอินพุตเป็นพัลส์แสงที่จะนำเข้าไปในระบบสามชนิด ได้แก่ เกาส์เซียนพัลส์ โซลิตอนมืด และโซลิตอนสว่าง โดยใช้พารามิเตอร์ที่เหมาะสม

การจำลองนี้ใช้ระบบโพรงสั่นพ้องวงแหวนสองรูปแบบ โดยแต่ละระบบจะรับอินพุตสามรูปแบบ ทั้งสองระบบประกอบด้วยตัวกรองแอด/ดรอปหนึ่งตัว โดยระบบแรกจะมีวงแหวนสั่นพ้องสองวง ส่วนระบบที่สองจะมีวงแหวนสั่นพ้องสามวง ผลที่ได้จากทั้งสองระบบคือโซลิตอนสว่างสำหรับอินพุตทั้งสามแบบ อย่างไรก็ตาม ระบบแรกจะให้โซลิตอนสว่างที่ทรูพุตพอร์ตเท่านั้น ส่วนระบบที่สองจะให้โซลิตอนสว่างทั้งที่ทรูพุตพอร์ตและดรอปพอร์ต

สิ่งที่น่าสนใจที่สุดคือโซลิตอนสว่างที่ได้จากระบบโพรงสั่นพ้องวงแหวนโดยนำเข้าเกาส์เซียนพัลส์ซึ่งสามารถนำไปทำเป็นตัวสร้างโซลิตอนสว่างจากลำแสงเลเซอร์ได้

คำสำคัญ : เกาส์เซียนพัลส์ โซลิตอนมืด โซลิตอนสว่าง โพรงสั่นพ้องวงแหวน

Thesis Title	Mathematical Simulation of Light Pulse Propagating within a Microring Resonator System
Student name	Mr. Buddhaporn Vanishkorn
Student ID	52650202
Degree	Doctor of Philosophy (Applied Mathematics)
Department	Mathematics
Year	2015
Thesis Advisor	Associate Professor Dr. Puntani Pongsumpun (Acting in place of thesis advisor)

Abstract

In this thesis, we use mathematical simulation to study the results of light pulse propagating within a ring resonator system. The inputs are light pulses of three forms: the Gaussian pulse, the dark soliton and the bright soliton, using the suitable simulation parameters.

The simulation employs two different ring resonator systems. Each system accepts all three forms of inputs. Both systems have one add/drop filter. The first system has two ring resonators while the second system has three. Both systems give bright solitons, for all types of inputs. However, in the first system, the bright solitons are detected from the throughput port only while in the second system, the bright solitons are detected from both the throughput port and the drop port.

The most interesting result is the bright soliton pulses from ring resonator systems by using the Gaussian pulse input, which can be used to produce the bright soliton generator from a laser pulse.

Keywords: Gaussian pulse, dark soliton, bright soliton, ring resonator

Acknowledgements

I would like to express my sincere gratitude to my advisor, Associate Professor Dr. Preecha Yupapin, for giving me an opportunity to do this research, for providing me all support and guidance, and for his understanding, patience and encouragement till the completion of the research.

I respect and deeply appreciate Associate Professor Dr. Puntani Pongsumpun for her helpful advices for invaluable comments for this research.

I am fully indebted to my committees, Assistant Professor Dr. Jaipong Kasemsuwan, Assistant Professor Dr. Atid Kangtunyakarn and Assistant Professor Dr. Wichai Witayakittilerd, for their helpful comments. I also heartily thank my external examiner, Dr. Yos Sompornjaroensuk for his kindness.

I gratefully acknowledge funding provided by King Mongkut's Institute of Technology Ladkrabang.

I greatly appreciate all lecturers and staffs in Department of Mathematics, Faculty of Science, King Mongkut's Institute of Technology Ladkrabang. Especially to Dr. Kampanat Namngam and Assistant Professor Dr. Nopparat Pochai for their assistance and suggestions and to Dr. Kannanut Chamsri for her helping and giving me words of encouragement.

In addition, I am grateful for Associate Professor Dr. Preecha Yupapin's students: Dr. Chat Teeka and Mr. Keerayoot Srinuanjan, and others person for suggestions and all their help.

Finally, I would like to thank my family and my friends for their love, goodwill and support.

Mr. Buddhaporn Vanishkorn

Table of Contents

Table of Contents (Continued)

List of Tables

Table **page**

List of Figures

Figure **Page**

List of Figures (Continued)

Figure **Page**

List of Figures (Continued)

Figure **Page**

Symbols

Symbol **Page**

Chapter I

Introduction

1.1 Statement and Significant of the Problems

Fibre optic networks are the backbone of communication systems, they can send and receive data in high speed rate. One technique is the fibre transmission capacity using different transmission wavelengths at the same time, this technique is called “Wavelength division multiplexing” (WDM) [1].

For example WDM filter devices:

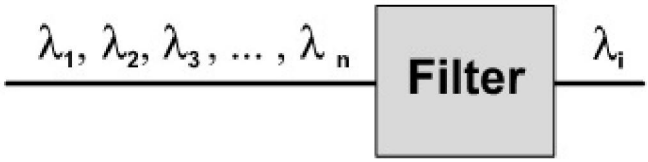

Figure 1.1 Band pass filter which selects the desired channel [1].

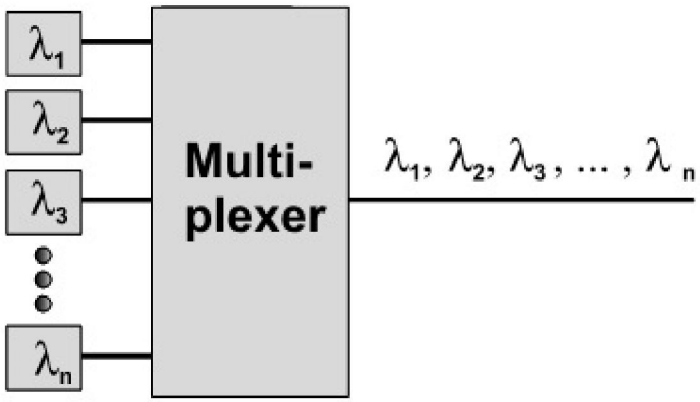

Figure 1.2 The Multiplexer combines sources with different wavelengths into a single output. In reverse direction, the structure is used as demultiplexer [1].

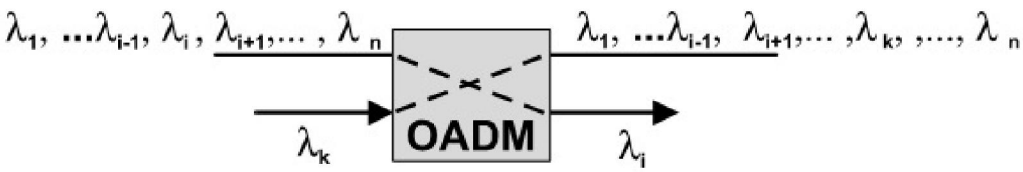

Figure 1.3 Optical add-drop multiplexer where channel λ_k is added to and channel λ_i is dropped from the WDM spectrum [1].

The WDM communication systems require optical components, and therefore a Gaussian pulse was used. The Gaussian pulse has been recognized in the form of a laser pulse, and so the Gaussian pulse generator is very low cost. However, the laser pulse has some problems, i.e. the high output power or long distance. Optical soliton came to be a powerful tool that can overcome some of these problems. The non-dispersion of soliton in medium is an advantage. The solitons can naturally be divided into classes of dark soliton and bright soliton. The soliton generations and their behaviors are analyzed and described by Agarwal [2]. The solitons can be used as an information carrier in long distance high-speed optical transmissions.

1.2 Objectives of the study

The research aims to study the light pulses and the output of light pulse propagating within the ring resonator systems, and then design the ring resonator systems. After that, it studies and develops the mathematical simulation of the behaviors of light pulse propagation in the ring resonator systems.

1.3 Scopes of the study

Design the ring resonator systems in order to simulate the results which are obtained from the Gaussian pulse, bright soliton pulse and dark soliton pulse. The use of InGaAsP/InP as the fabricated material is proposed.

1.4 Process of the study

The process of the study following:

1) Study the Gaussian pulse, bright soliton pulse and dark soliton pulse.
2) Study the ratio between the output and input fields from a single ring resonator.
3) Study the ratio between the output and input fields from an add/drop filter.
4) Simulate the results from the ring resonator systems.
5) Discuss the results.

1.5 Benefits of the study

One can understand the processing of light pulse propagation with in the ring resonator. Furthermore, one can use the result of the three forms of laser pulses, such as Gaussian soliton, dark and bright soliton propagating within the proposed ring resonator systems for signal transmission. Moreover, it is used to encode signal in fibre optic communications.

Chapter II

Pulse Propagation and Ring Resonator

This chapter contains the knowledge of pulse propagating in waveguide and ring resonator.

2.1 The optical field and loss in propagation

The optical field is used in physics and vector calculus to designate the electric field shown as E in the electromagnetic wave equation which can be derived from Maxwell's Equations. In electromagnetic theory, the electromagnetic wave propagates such that both the magnetic field oscillation and the electric field oscillation are perpendicular to the direction of propagation of the wave. As with any wave, the electromagnetic wave carrier energy, thus the total energy density is shared between the constituent electric and magnetic fields. Since the electric field is well more effective at exerting forces and doing work on charges than the magnetic field, the electric field E is assigned to as the optical field [3].

Optical power (P) is the degree to which a lens, mirror, or other optical system converges or diverges light. It is equal to the correlative of the focal length of the device. High optical power accords to short focal length. The SI unit for optical power is the inverse metre (m^{-1}) [4].

Intensity (I) is the power translated per unit area, which is transmitted through a fabricated surface perpendicular to the propagation direction. In the SI system, it has unit's watts per square metre (W/m^2). It is used most frequently with waves (e.g. sound or light), in which case the average power transfers over one period of the wave is used [5].

The intensity attenuation coefficient (α) is the gradual loss in intensity of any kind of flux through a medium. Attenuation in fiber optics, also known as transmission loss, is the contraction in intensity of the light beam (or signal) with respect to distance transited through a transmission medium. Attenuation coefficients in fiber optics usually use units of dB/km through the medium mature to the

relatively high aspect of transparency of modern optical transmission media. The attenuation coefficient is a portion that characterizes how easily a material or medium can be accessed by a beam of light, sound, particles, or other energy or matter. A large attenuation coefficient means that the beam is quickly "attenuated" as it passes through the medium, and a small attenuation coefficient means that the medium is relatively clear to the beam. The attenuation coefficient is the fellow of the penetration depth, and is measured in units of reciprocal length [6].

The insertion loss (γ) is the loss of signal power producing from the insertion of a device in a transmission line or optical fibre and is usually intended in decibels (dB) [7].

In electromagnetic theory, the phase constant, also called phase change constant, parameter or coefficient is the imaginary component of the propagation constant for a uniform wave. It expresses the change in phase per metre along the path moved by the wave at any instant and is equal to real part of the angular wavenumber of the wave. It is performed by the symbol k_n (The wave propagation number) and is measured in units of radians per metre. From the definition of wavenumber [8]

$$k_n = \frac{2\pi}{\lambda} = \frac{2\pi f}{v} = \frac{2\pi n}{vt}$$

where λ is the wavelength,

f is the frequency,

v is the velocity,

n is the event occurred,

t is the time.

Coupling is the adorable or undesirable transfer of energy from one medium, such as a metallurgic wire or an optical fiber, to another medium, entering fortuitous transfer. Coupling is also the shift of electrical energy from one circuit segment to another. For example, energy is transmitted from a power source to an electrical

load by means of conductive coupling, which may be either immune or hard-wire. An AC potential may be transmitted from one circuit segment to another having a DC potential by use of a capacitor. Electrical energy may be transmitted from one circuit segment to another segment with different impedance by use of a transformer. This is known as impedance matching. These are examples of electrostatic and electrodynamics inductive coupling. The coupling coefficient of resonators (κ) is a dimensionless value that characterizes communication of two resonators. Coupling coefficients are used in resonator filter theory. Resonators may be both electromagnetic and acoustic. Coupling coefficients well-adjudge with resonant frequencies and external quality factors of resonators are the generalized parameters of filters. In order to adjust the frequency lip of the filter, it is sufficient to optimize only these generalized parameters [9].

2.2 The Gaussian pulse

Lasers are sources of light with very special properties, as explained in the article on laser light. For that reason, there is a great variety of laser applications. The following sections award an overview.

In manufacturing, lasers are extensively used in manufacturing, e.g. for cutting, drilling, cladding, marking, soldering, ablating, surface treatment, engraving, micromachining, hardening, pulsed laser deposition, alignment, etc. In most cases, relatively high optical intensities are applied to a small spot, leading to intense heating, possibly evaporation and plasma generation. Essential aspects are the high spatial coherence of laser light, allowing for strong focusing, and often also the potential for generating intense pulses.

Laser processing methods have much leverage, compared with mechanical approaches. They grant the fabrication of very fine structures with high quality, avoiding mechanical stress such as caused by mechanical drills and blades. A laser beam with high beam quality can be used to drill very elegant and wide holes, e.g. for injection nozzles. A high processing speed is often managed, e.g. in the fabrication of filter sieves. Further, the lifetime limitation of mechanical tools is deleted. It can also be propitious to process materials without touching them.

In medical Applications, there is a wide bound of medical applications. Often these impart to the outer parts of the human body, which are easily compassed with light; examples are eye surgery and vision correction (LASIK), dentistry, dermatology and various kinds of cosmetic treatment such as tattoo removal.

Lasers are also used for surgery, exploiting the possibility to rip tissues while causing minimal bleeding. Very different types of lasers are required for medical applications, depending on the optical wavelength, output power, etc. In many cases, the laser wavelength is popular such that certain substances (e.g. pigments in tattoos or caries in teeth) absorb light more strongly than border tissue, so that they can be more precisely targeted. Medical lasers are not always used for cure. Some of them rather relief the diagnosis, e.g. via methods of ocular imaging, laser microscopy or spectroscopy.

In metrology, lasers are widely used in optical measure, e.g. for extremely precise position metrologies and optical surface profiling with interferometers, for long-distance range finding and exploration. Laser scanners are based on accumulated laser beams, which can read e.g. bar codes or other graphics over some distance. It is also possible to scan three-dimensional objects, e.g. in the background of crime scene investigation (CSI). Optical sampling is a technique applied for the impersonation of fast electronic microcircuits, microwave photonics, terahertz science, etc.

Lasers also grant for extremely precise time measurements and are therefore essential component of optical clocks which are beginning to outperform the directly used cesium atomic clocks. Fibre-optic sensors, often probed with laser light, allow for the divided measurement of temperature, stress, and other quantities e.g. in oil pipelines and wings of airplanes [10].

A Gaussian pulse has a characteristic symmetric bell curve shape, the Gaussian pulse can be represented by a laser pulse. It is in the form

$$E(t) = Ae^{-(t-t_0)^2} \tag{2.1}$$

where A is the amplitude,

t_0 is the center of curve.

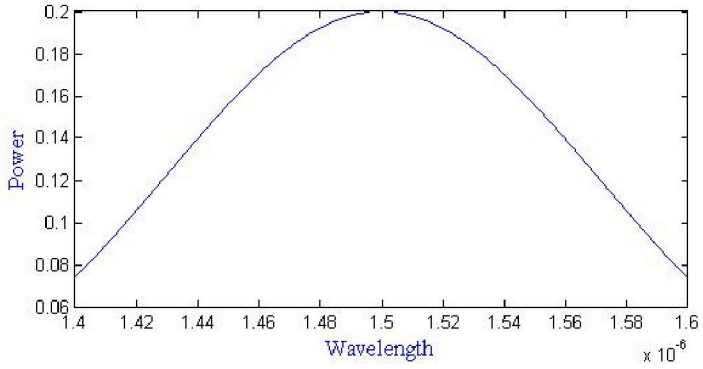

Figure 2.1 The Gaussian pulse of wavelength.

2.3 The soliton pulses

In this section, we introduce soliton pulses, the solitons are caused by a cancellation of nonlinear and dispersive effects in the medium, which there are two different soliton pulses for this thesis.

An optical soliton is a pulse that propagates without distortion due to dispersion or other effects. They are a nonlinear phenomenon caused by self-phase modulation (SPM) which means that the electric field of the wave changes the index of refraction viewed by the wave (Kerr effect). SPM causes a red shift at the leading edge of the pulse. Solitons obtain when this shift is removed due to the blue shift at the leading edge of a pulse in a region of anomalous dispersion, resulting in a pulse that retains its shape in both frequency and time. Solitons are therefore an essential development in the field of optical communications [11].

2.3.1 The bright soliton pulse

A bright soliton is characterized as a localized intensity peak above a continuous wave background, it for which the incident field is of the form

$$E(t) = E_0 \operatorname{sec h}\left[\frac{T}{T_0}\right] e^{\frac{z}{2L_D} - i\omega_0 t} \tag{2.2}$$

where E_0 is the constant light field amplitude,

T is the soliton pulse propagation time in a frame moving at the group velocity,

T_0 is the soliton pulse propagation time at initial input,

z is the propagation distance,

L_D is the dispersion length of the soliton pulse,

ω_0 is the frequency shift of the soliton,

t is the soliton phase shift time.

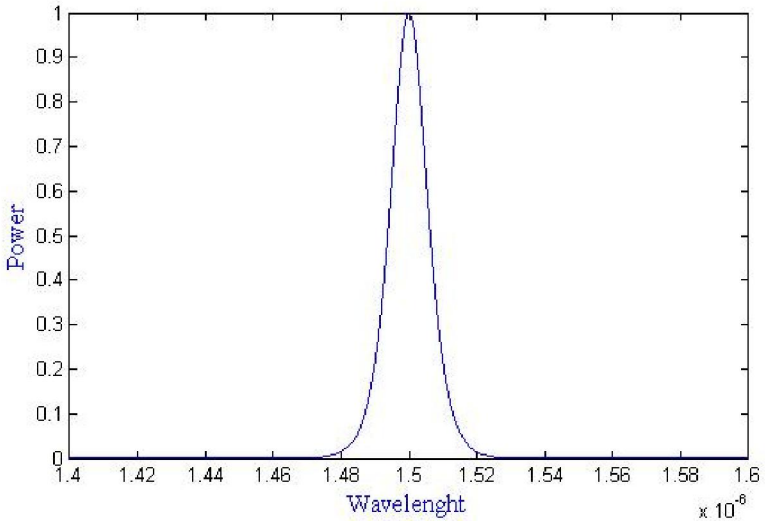

Figure 2.2 The bright soliton pulse.

2.3.2 The dark soliton pulse

A dark soliton pulse is featured as a localized intensity plunge below a continuous wave background, it for which the incident field is of the form

$$E(t) = E_0 \tan \mathrm{h}\left[\frac{T}{T_0}\right] e^{\frac{z}{2L_D} - i\omega_0 t} \tag{2.3}$$

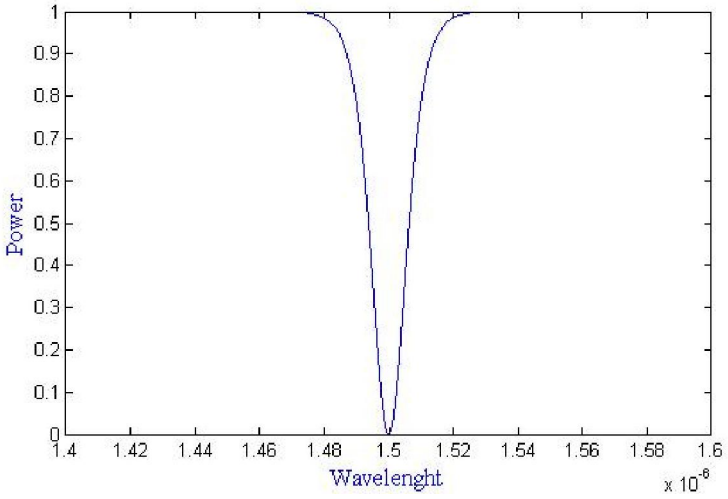

Figure 2.3 The dark soliton pulse.

2.4 The refractive index

The refractive index is a dimensionless number that depicts how light, or any other radiation, propagates through that medium. The refractive index ranges with the wavelength of light. This is called dispersion and causes the rifting of white light into its constituent colors in prisms and rainbows, and chromatic aberration in lenses. Light propagation in absorbing materials can be depicted using a complex valued refractive index. The imaginary part then holds the attenuation, while the real part accounts for refraction [12]. It is given by

$$n = n_0 + n_2 I = n_0 + n_2 \left(\frac{P}{A_{eff}} \right) \tag{2.4}$$

where n_0 is linear refractive index,

n_2 is nonlinear refractive index,

I is optical intensity,

P is optical power,

A_{eff} is effective mode core area of the device.

2.5 The light pulse propagations

2.5.1 Waveguide

A waveguide is a structure that guides waves, such as electromagnetic waves or sound waves. There are different types of waveguides for each type of wave. The wave guide in this thesis is called “optical waveguide”. The light pulse propagating in the line wave guide has the relation of throughput port optical field and input light field shown in Eq. (2.5), the arrow show the direction of optical field

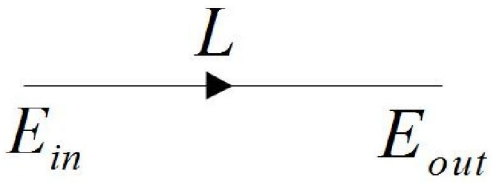

Figure 2.4 The optical field travelling within waveguide.

$$E_{out} = E_{in} e^{-\frac{\alpha}{2} z - i k_n z} \tag{2.5}$$

where E_{out} is the optical fields of the throughput,

E_{in} is the input light field,

α is the intensity attenuation coefficient of waveguide $0 \le \alpha \le 1$,

k_n is the wave propagation number in a vacuum,

L is the waveguide length.

2.5.2 Coupler

A fibre coupler is a four-port device subsisting of two fibres that have been fused together, etched, or polished over a small interaction region [3].

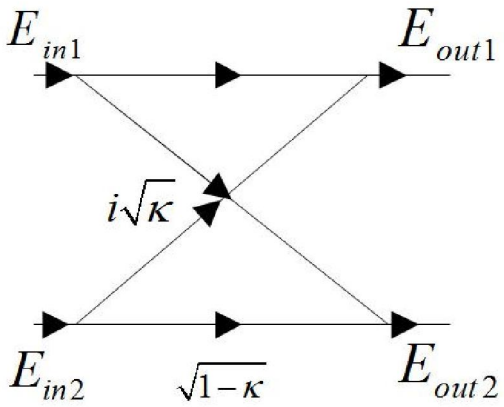

Figure 2.5 The optical fields coupling.

$$E_{out1} = \sqrt{1-\gamma}\left(E_{in1}\sqrt{1-\kappa} + E_{in2}\, i\sqrt{\kappa}\right) \tag{2.6}$$

$$E_{out2} = \sqrt{1-\gamma}\left(E_{in2}\sqrt{1-\kappa} + E_{in1}\, i\sqrt{\kappa}\right) \tag{2.7}$$

where γ is the intensity insertion loss coefficient of coupler $0 \le \gamma \le 1$,

κ is the amplitude coupling coefficient of the coupling region $0 \le \kappa \le 1$.

2.6 The ring resonator

2.6.1 The single ring resonator

An optical ring resonator is a set of waveguides in which at least one is a closed loop coupled to some kind of light input and output. The concepts abaft optical ring resonators are the same as those behind whispering galleries except that they use light and follow the properties behind effective interference and total internal reflection. When light of the resonant wavelength is travelled through the loop from input waveguide, it makes up in intensity over multiple round-trips due to constructive interference and is output to the output bus waveguide which deal as a detector waveguide. Because only a select few wavelengths will be at resonance within the loop, the optical ring resonator functions as a filter. Additionally, as implied earlier, two or more ring waveguides can be coupled to each other to form an add/drop optical filter. Critical to explaining how an optical ring resonator works, is the comprehension of how the linear waveguides are coupled to the ring waveguide. When a beam of light passes through a wave guide as shown in the graph on the right, part of light will be coupled into the optical ring resonator. The logic for this phenomenon to happen is because the wave property of the light, or if we consider it in ray optics, it is because of the transportation effect. In other words, if the ring and the waveguide are close enough, the light in the waveguide will be translated into the ring. There are three aspects that disturb the optical coupling: the distance, the coupling length and the refractive indices between the waveguide and the optical ring resonator. In order to optimize the coupling, it is usually the case to slim the distance between the ring resonator and the waveguide. The closer the distance, the easier the optical coupling happens. In addition, the coupling length affects the coupling as well. The coupling length represents the effective curve length of the ring resonator for the coupling aspect to happen with the waveguide. It has been studied that as the optical coupling length increases, the difficulty for the coupling to happen decreases. Furthermore, the refractive index of the waveguide material, the ring resonator material and the medium material in between the waveguide and the ring resonator also perturb the optical coupling. The medium material is usually the important one been studied since it has a great effect on the translation of the light

wave. The refractive index of the medium can be either large or small concord to various applications and purposes [13].

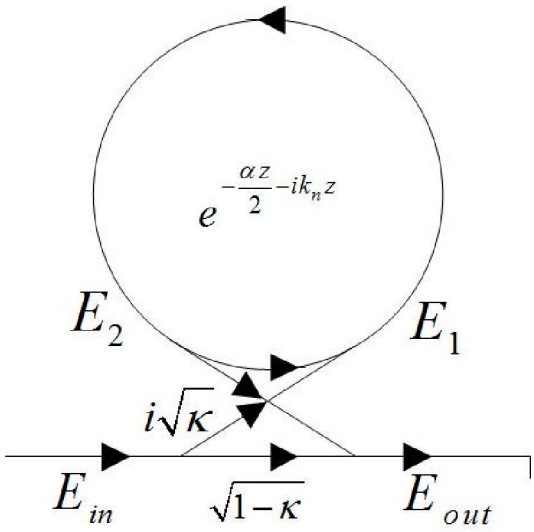

Figure 2.6 The optical field travelling in the ring resonator [6].

When the optical field propagating in the ring resonator, the optical field can calculate by Eq. (2.6), (2.7) and (2.5), so

$$E_1 = \sqrt{1-\gamma}\left(E_{in}\, i\sqrt{\kappa} + E_2\sqrt{1-\kappa}\right) \tag{2.8}$$

$$E_{out} = \sqrt{1-\gamma}\left(E_2\, i\sqrt{\kappa} + E_{in}\sqrt{1-\kappa}\right) \tag{2.9}$$

$$E_2 = E_1\, e^{-\frac{\alpha}{2}z-ik_n z} \tag{2.10}$$

therefore

$$E_1 = \sqrt{1-\gamma}\left(E_{in}\, i\sqrt{\kappa} + E_1\sqrt{1-\kappa}\, e^{-\frac{\alpha}{2}z-ik_n z}\right)$$

$$E_1 = \frac{\sqrt{1-\gamma}\, E_{in}\; i\sqrt{\kappa}}{1-\sqrt{1-\gamma}\sqrt{1-\kappa}\, e^{-\frac{\alpha}{2}z-ik_n z}}$$

Substitute E_1 in Eq. (2.10), so

$$E_2 = \frac{\sqrt{1-\gamma}\, E_{in}\, i\sqrt{\kappa}\, e^{-\frac{\alpha}{2}z-ik_n z}}{1-\sqrt{1-\gamma}\sqrt{1-\kappa}\, e^{-\frac{\alpha}{2}z-ik_n z}}$$

Substitute E_2 in Eq. (2.9), therefore

$$E_{out} = \sqrt{1-\gamma}\left[\left(\frac{\sqrt{1-\gamma}\, E_{in}\, i\sqrt{\kappa}\, e^{-\frac{\alpha}{2}z-ik_n z}}{1-\sqrt{1-\gamma}\sqrt{1-\kappa}\, e^{-\frac{\alpha}{2}z-ik_n z}}\right) i\sqrt{\kappa} + E_{in}\sqrt{1-\kappa}\right]$$

$$E_{out} = E_{in}\sqrt{1-\gamma}\left(\frac{\sqrt{1-\kappa}-\sqrt{1-\gamma}\,e^{-\frac{\alpha}{2}z-ik_n z}}{1-\sqrt{1-\gamma}\sqrt{1-\kappa}\,e^{-\frac{\alpha}{2}z-ik_n z}}\right)$$

$$\frac{E_{out}}{E_{in}} = \sqrt{1-\gamma}\left(\frac{\sqrt{1-\kappa}-\sqrt{1-\gamma}\,e^{-\frac{\alpha}{2}z-ik_n z}}{1-\sqrt{1-\gamma}\sqrt{1-\kappa}\,e^{-\frac{\alpha}{2}z-ik_n z}}\right)$$

$$\frac{\left|E_{out}\right|^2}{\left|E_{in}\right|^2} = (1-\gamma)\left(\frac{1-\kappa-2\sqrt{1-\gamma}\sqrt{1-\kappa}\,e^{-\frac{\alpha}{2}z}\cos(k_n z)+(1-\gamma)e^{-\alpha z}}{1-2\sqrt{1-\gamma}\sqrt{1-\kappa}\,e^{-\frac{\alpha}{2}z}\cos(k_n z)+(1-\gamma)(1-\kappa)e^{-\alpha z}}\right) \quad (2.11)$$

The ratio between the output and input fields in single ring resonator, which can be expressed as

$$\frac{\left|E_{out}\right|^2}{\left|E_{in}\right|^2} = (1-\gamma)\left[1-\frac{\left(1-(1-\gamma)e^{-\alpha z}\right)\kappa}{\left(1-e^{-\frac{\alpha z}{2}}\sqrt{1-\gamma}\sqrt{1-\kappa}\right)^2+4e^{-\frac{\alpha z}{2}}\sqrt{1-\gamma}\sqrt{1-\kappa}\sin^2\left(\frac{\phi}{2}\right)}\right] \quad (2.12)$$

Where $\phi = k_n z$ is the phase.

2.6.2 The add/drop filter

An optical add/drop multiplexer is a device used in wavelength-division multiplexing systems for multiplexing and routing different channels of light into or out of a single mode fibre. This is a type of optical node, which is generally used for the conception of optical telecommunications networks. "Add" and "drop" here refer to the capability of the device to add one or more new wavelength channels to an existing multi-wavelength WDM signal, and/or to drop (remove) one or more channels, passing those signals to another network passage. An optical add-drop multiplexer may be considered to be a special type of optical cross-connect [14].

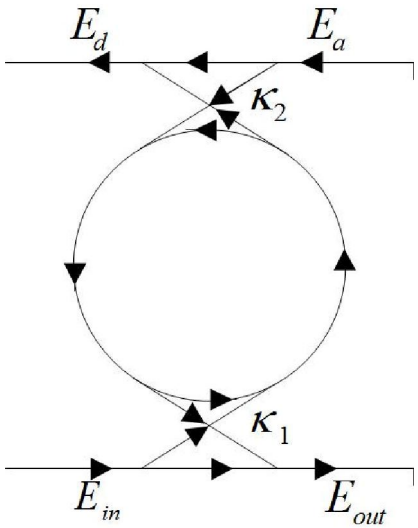

Figure 2.7 The optical field travelling in the add/drop filter [6].

Assume that $E_a = 0$, the ratio between the output and input fields in add/drop filter, which can be expressed as

$$\frac{|E_{out}|^2}{|E_{in}|^2} = \frac{(1-\kappa_1) - 2\sqrt{1-\kappa_1}\sqrt{1-\kappa_2}\,e^{-\frac{\alpha z}{2}}\cos\phi + (1-\kappa_2)e^{-\alpha z}}{1+(1-\kappa_1)(1-\kappa_2)e^{-\alpha z} - 2\sqrt{1-\kappa_1}\sqrt{1-\kappa_2}\,e^{-\frac{\alpha z}{2}}\cos\phi} \tag{2.13}$$

$$\frac{|E_d|^2}{|E_{in}|^2} = \frac{\kappa_1\kappa_2 e^{-\frac{\alpha z}{2}}}{1+(1-\kappa_1)(1-\kappa_2)e^{-\alpha z} - 2\sqrt{1-\kappa_1}\sqrt{1-\kappa_2}\,e^{-\frac{\alpha z}{2}}\cos\phi} \tag{2.14}.$$

Chapter III

The System of Ring Resonators

This chapter contains the method to design some systems of ring resonator. In this thesis, we use the mathematical simulation to show the behaviors of light pulse propagating within the microring resonator. The material used is InGaAsP / InP. The light pulses used in this research are three different forms: Gaussian pulse, bright and dark soliton pulses.

The ring resonators in the system have size in micrometre, it's called "the microring resonator". In this thesis, the author fixed some parameters for the ring resonators system.

3.1 The first system: two ring resonators and an add/drop filter

The first system contained two ring resonators and an add/drop filter, which R_1 , R_2 and R_d are ring radii in micrometre scale. The light pulse input (E_{in}) travel from R_1 to R_2 and then R_d . The light pulse output are E_t and E_d . The second ring resonator (R_2) has accelerated the resonance of light pulse, and the add/drop filter have filter the light pulse.

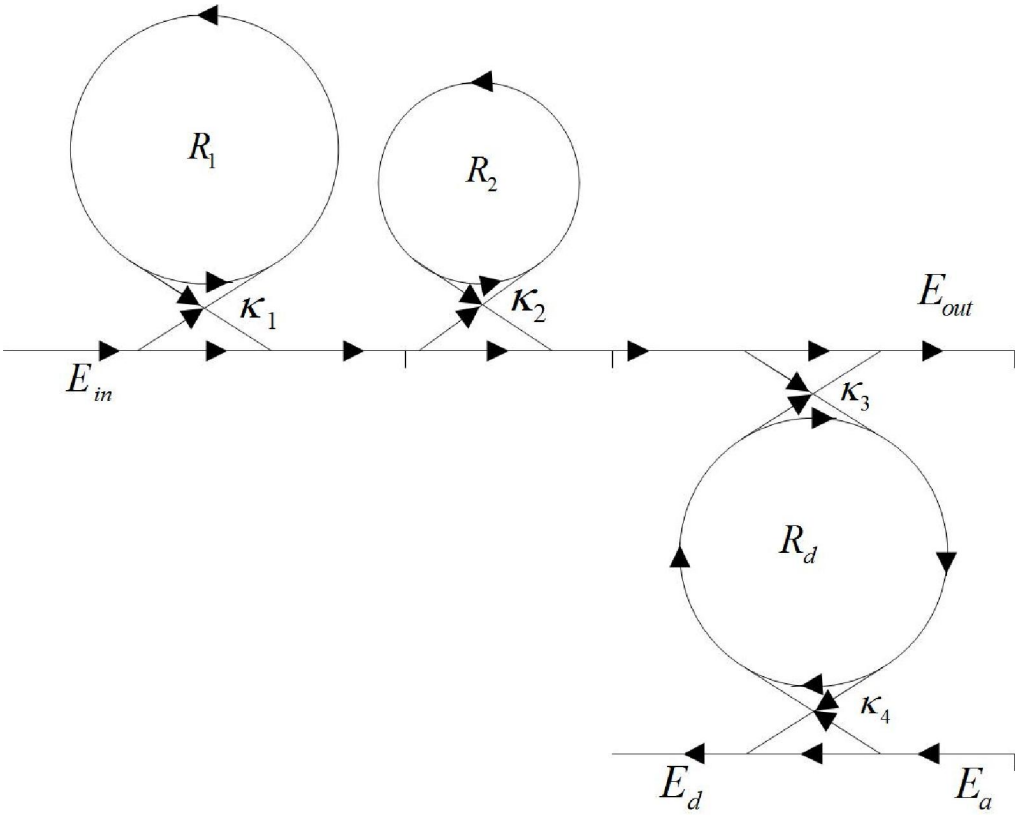

Figure 3.1 The first system of ring resonator.

We will split the considered system into 3 stages.

Stage 1: we can obtain E_{R1} from E_{in} by ring R_1 (shown in Fig. 3.1.1).

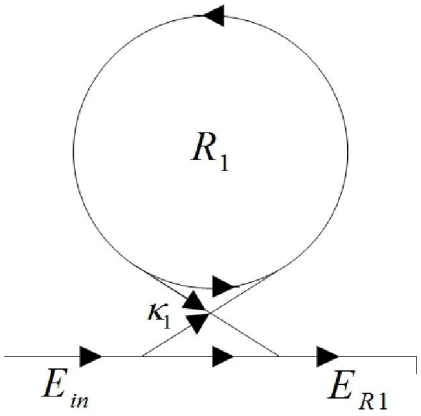

Figure 3.2 The ring R_1 in first system.

Stage 2: we will input the E_{R1} into the ring R_2 (shown in Fig. 3.1.2).

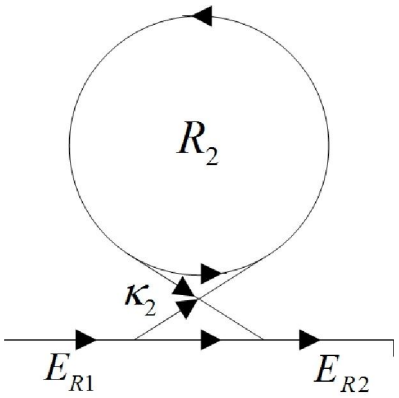

Figure 3.3 The ring R_2 in first system.

Stage 3: this stage the input is E_{R2} travelling into ring R_d . It given two outputs, there are E_{out} and E_a (shown in Fig. 3.1.3).

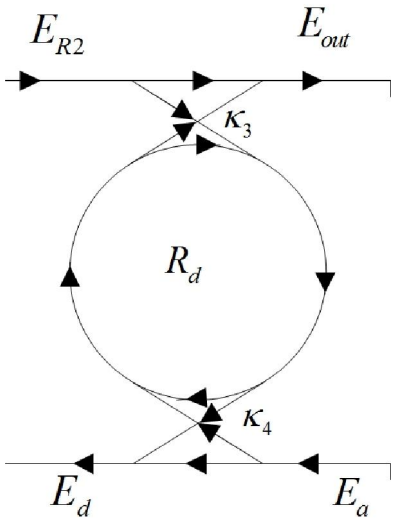

Figure 3.4 The ring(add/drop filter) R_d in first system.

3.2 The second system: three ring resonators and add/drop filter

The second system contained three ring resonators and an add/drop filter. The light pulse travelling same as the first system.

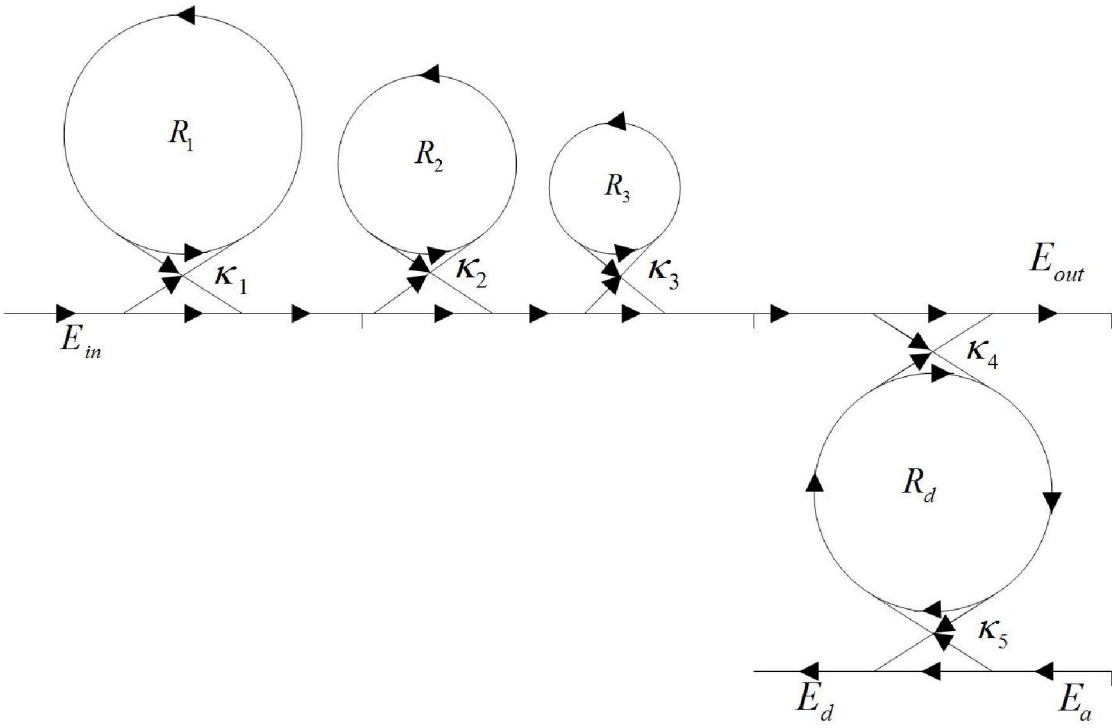

Figure 3.5 The second ring resonator system.

We have 4 stages in this system, it propagations similarly the first system.

Chapter IV

The Generating of Bright Solitons

This chapter contains the results of light pulse propagating from the first and second systems in chapter 3.

We will propose the simulation into 3 cases. The input pulses are different:

1. Gaussian pulse

2. bright soliton pulse

3. dark soliton pulse.

4.1 The outputs of first system

In this section, we get the results of light propagating from the first system in chapter 3, the results of three type light pulse inputs are the bright soliton at throughput port of first system.

The parameters for the first system are used, ring radii R_1 = 16 μm, R_2 = 5.0 μm, and R_d = 25.0 μm, linear refractive index n_0 = 3.34 (InGaAsP/InP), the nonlinear refractive index n_2 =2.2x10^{-17} m^2/W, effective mode core area A_{eff} = 0.50 μm^2 and 0.25 μm^2 for a microring resonator and add/drop filter, respectively, intensity attenuation coefficient α = 0.5 dB mm^{-1}, insertion loss γ = 0.1, coupling coefficient κ_1 =0.55, κ_2 =0.7, $\kappa_3 = \kappa_4$ =0.9, and setting E_a = 0 (no add the light pulse into add port)

Ring	R_1	R_2	R_d	n_0	n_2	A_{eff}	α	γ	κ_1	κ_2	κ_3	κ_4
R_1	16	-	-	3.34	2.2x10^{-17}	0.5	0.5	0.1	0.55	-	-	-
R_2	-	5	-	3.34	2.2x10^{-17}	0.5	0.5	0.1	-	0.7	-	-
R_d	-	-	25	3.34	2.2x10^{-17}	0.25	0.5	0.1	-	-	0.9	0.9

Table 4.1 the table of parameters for first system.

4.1.1 The output by using the Gaussian pulse as the input port

The Gaussian pulse with center wavelength (λ_0) at 1.55 μm, peak power at 1W/m^2 is input into the system as shown in Fig. 4.1.

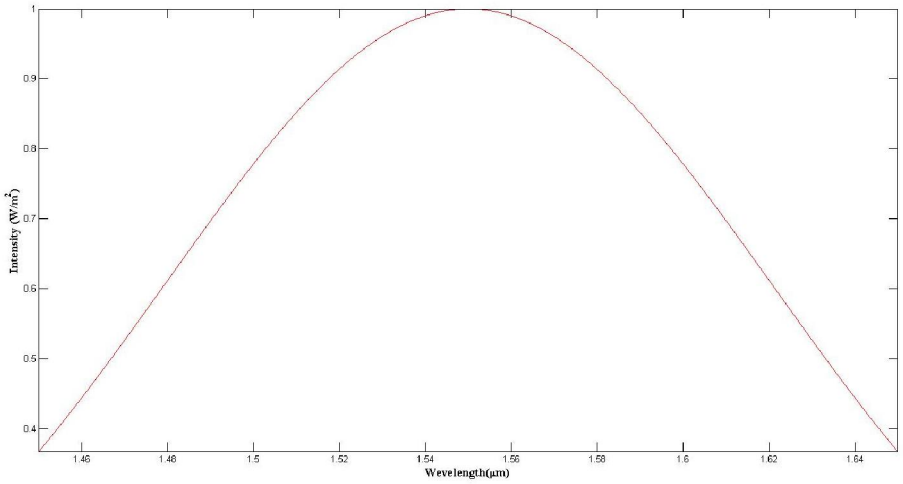

Figure 4.1 Gaussian pulse input E_{in} for first system.

The first stage (R_1), when the Gaussian pulse travelling in the ring resonator R_1 , we get the E_{R1} from the first ring R_1.

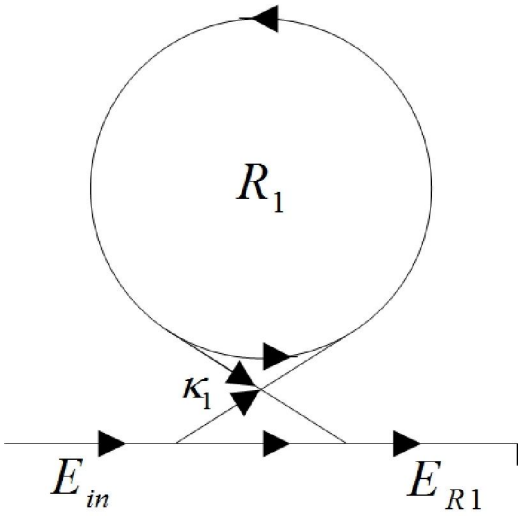

Figure 4.2 The ring R_1.

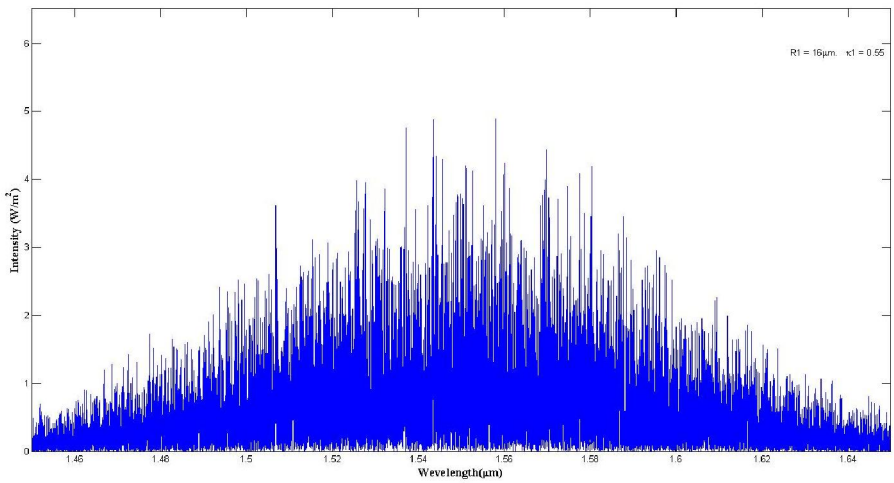

Figure 4.3 Output E_{R1} from ring R_1.

In this stage, the output power increase from 1W/m^2 to 5W/m^2.

Second stage (R_2), we get the E_{R2} from the second ring R_2 .

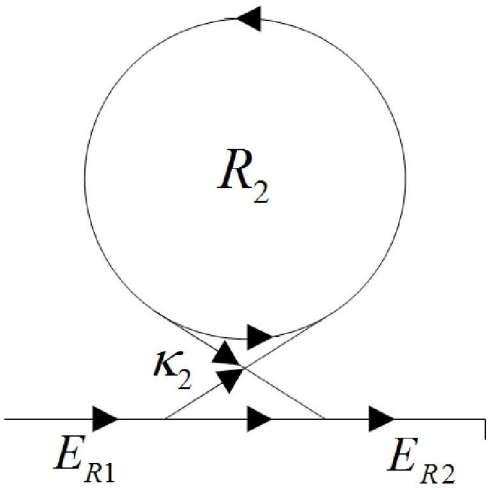

Figure 4.4 The ring R_2 .

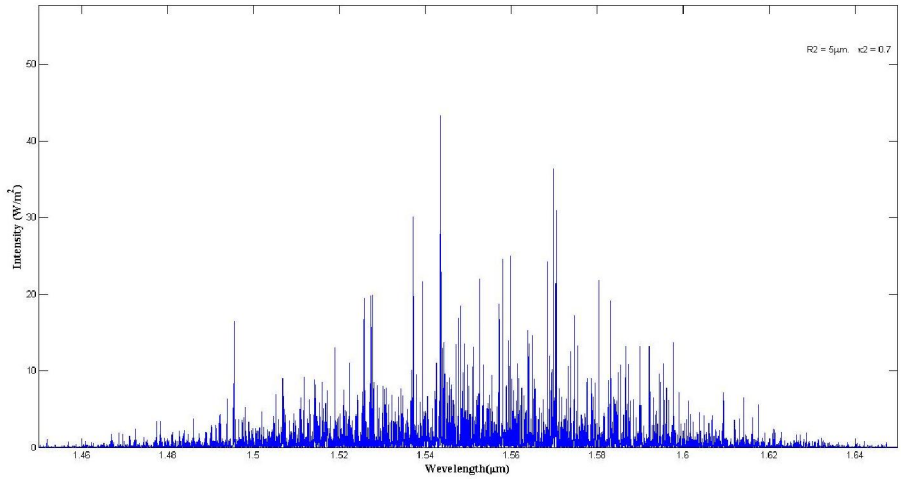

Figure 4.5 Output E_{R2} from ring R_2 .

This stage, the output power increase from 5W/m^2 to 45W/m^2.

Final stage in the first system for the Gaussian pulse input (R_d), we get two outputs from the add/drop filter R_d , there are the E_{out} and E_d .

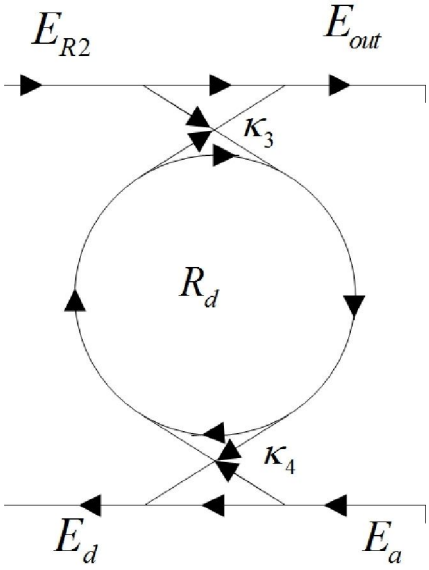

Figure 4.6 The add/drop filter R_d .

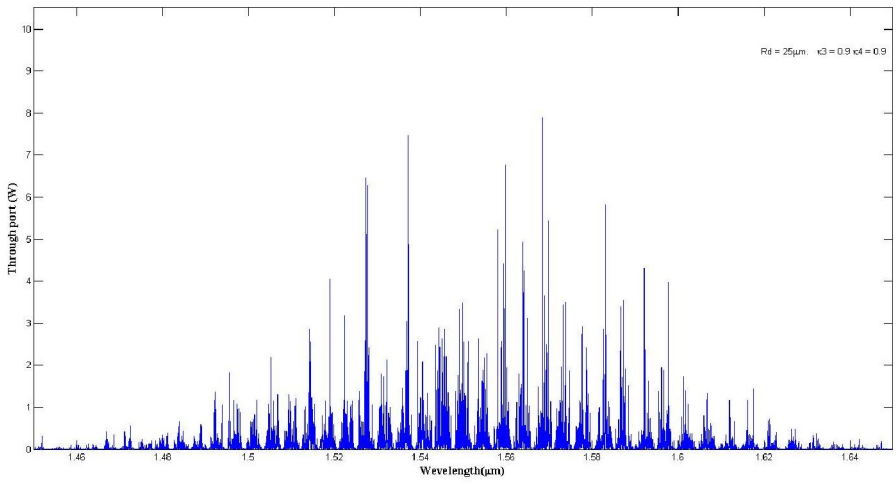

Figure 4.7 Output E_{out} at throughput port form add/drop filter R_d .

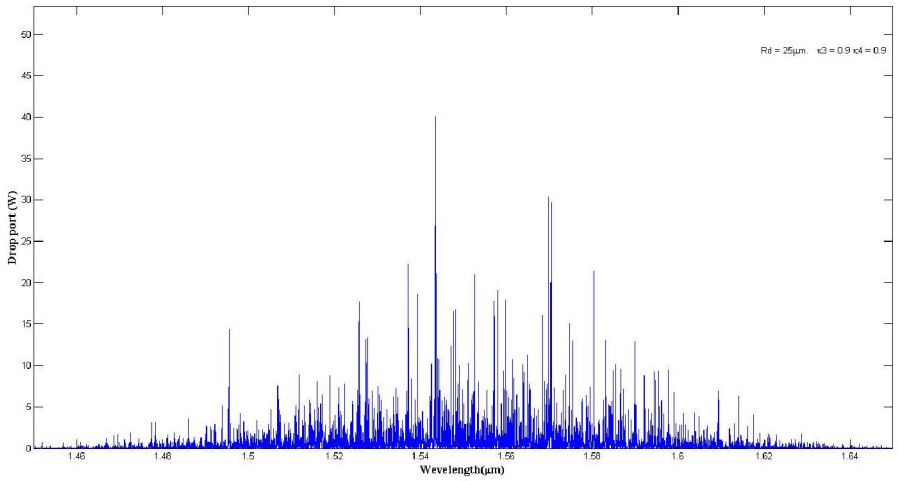

Figure 4.8 Output E_d at drop port form add/drop filter R_d.

This stage, the throughput port has the output power at 8 W/m^2 and drop port can divide the excess power at 40 W/m^2. The output at throughput port is the bright solitons.

4.1.2 The output by using the bright soliton pulse as the input port

The bright soliton pulse with center wavelength (λ_0) at 1.55 μm, peak power at 1W/m^2 is input into the system as shown in Fig. 4.5.

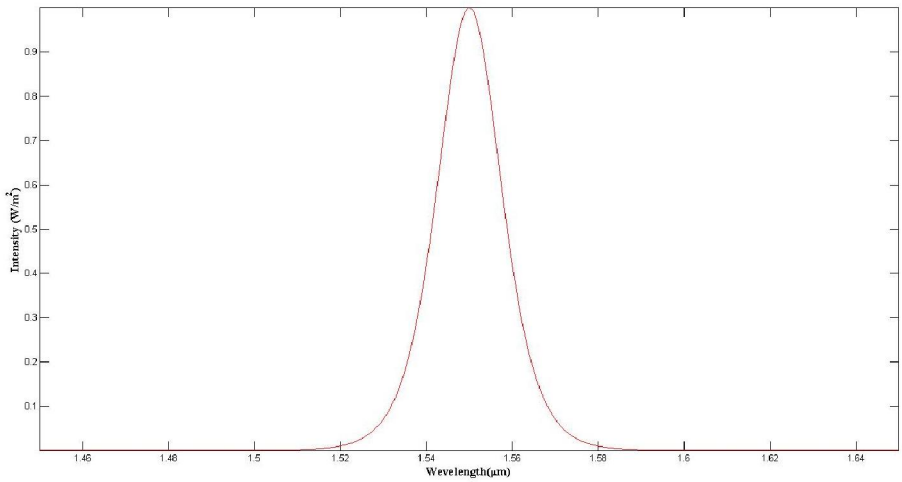

Figure 4.9 The bright soliton pulse input E_{in} for first system.

Stage 1 (R_1), we get the E_{R1} from the first ring R_1.

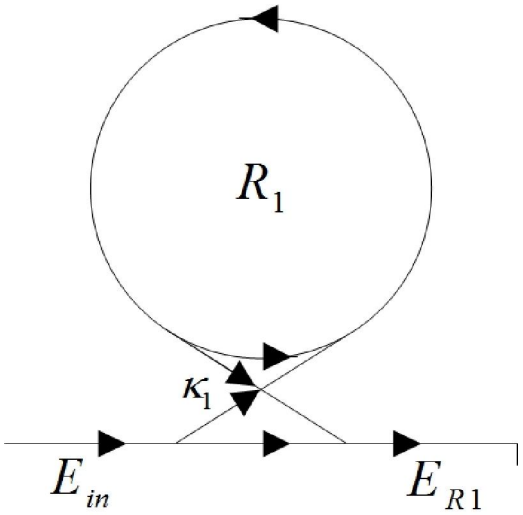

Figure 4.10 The ring R_1.

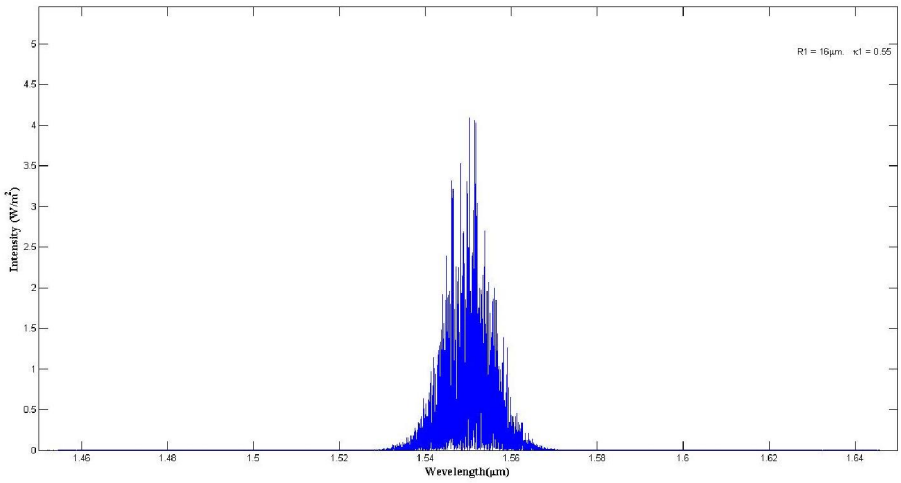

Figure 4.11 Output E_{R1} from ring R_1.

In this stage, the output power increase from 1W/m^2 to 4.5W/m^2.

Stage 2 (R_2), we get the E_{R2} from the second ring R_2 .

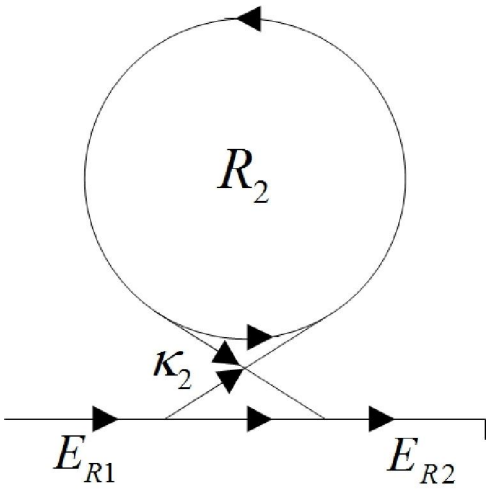

Figure 4.12 The ring R_2 .

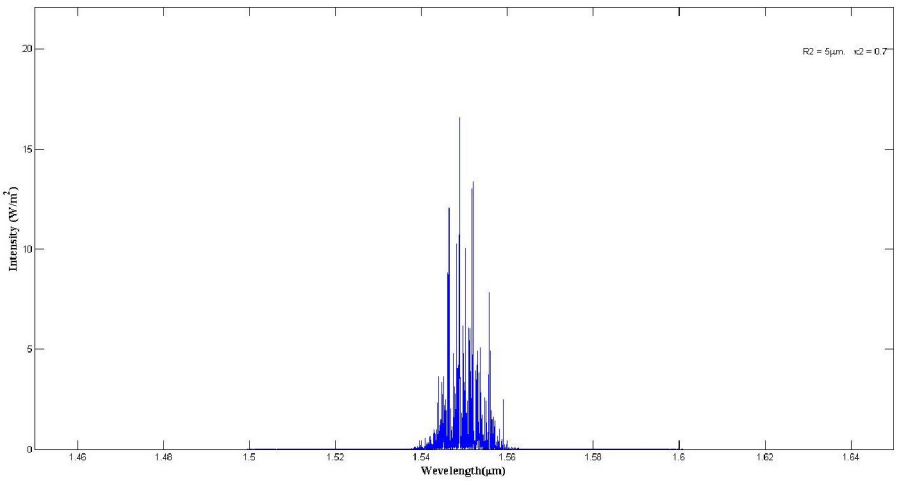

Figure 4.13 Output E_{R2} from ring R_2 .

This stage, the output power increase from 4.5W/m^2 to 17W/m^2.

Stage 3(R_d), the outputs of the first system by using the bright soliton pulse input, we get two outputs from the add/drop filter R_d, there are the E_{out} and E_d .

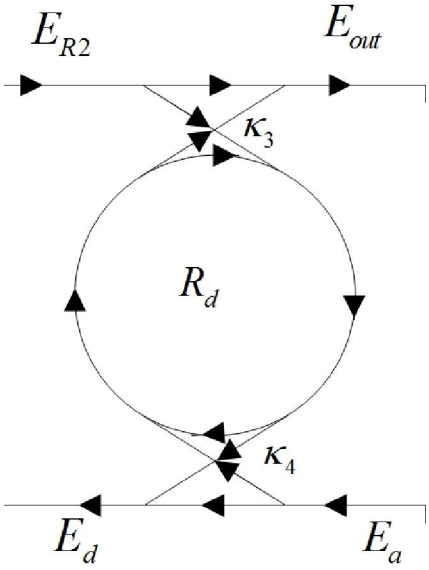

Figure 4.14 The add/drop filter R_d.

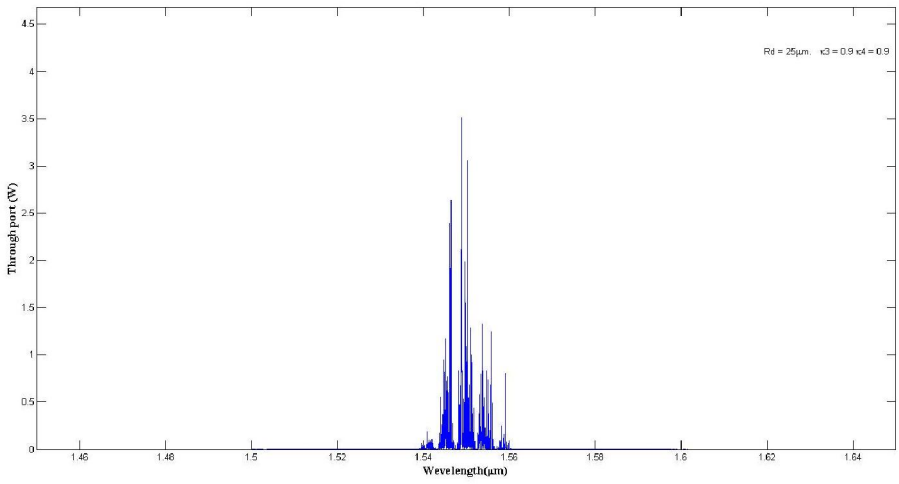

Figure 4.15 Output E_{out} at throughput port form add/drop filter R_d.

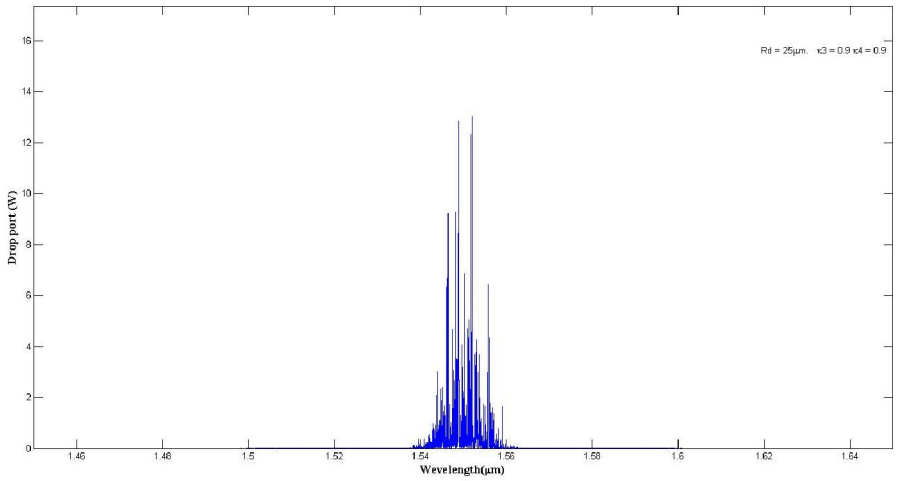

Figure 4.16 Output E_d at drop port form add/drop filter R_d.

In this case, we get the bright solitons at throughput and drop ports. The increasing of power similarly the Gaussian pulse. The throughput port has the output power at 3.5 W/m^2 and drop port can divide the excess power at 13 W/m^2.

4.1.3 The output by using the dark soliton pulse as the input port

The dark soliton pulse with center wavelength (λ_0) at 1.55 μm, peak power at 1W/m^2 is input into the system as shown in Fig. 4.9.

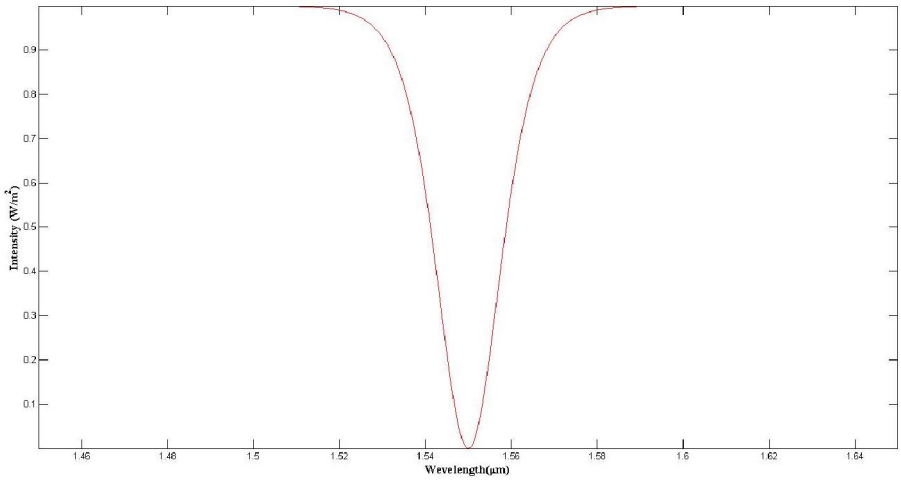

Figure 4.17 The dark soliton pulse input E_{in} for first system.

Stage 1 (R_1), we get the E_{R1} from the first ring R_1.

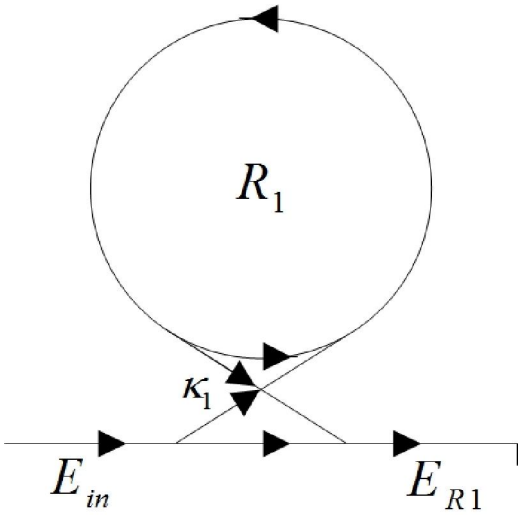

Figure 4.18 The ring R_1.

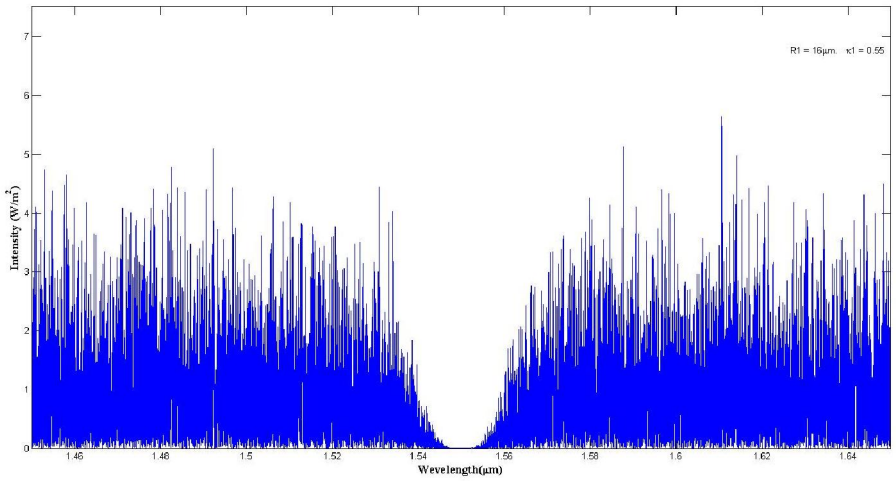

Figure 4.19 Output E_{R1} from ring R_1.

In this stage, the output power increase from 1W/m^2 to 6W/m^2.

Stage 2 (R_2), we get the E_{R2} from the second ring R_2 .

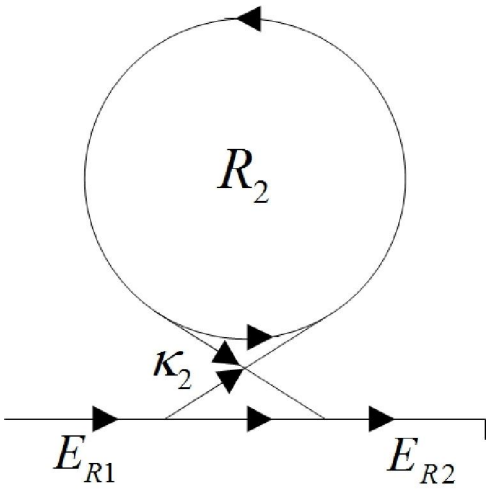

Figure 4.20 The ring R_2 .

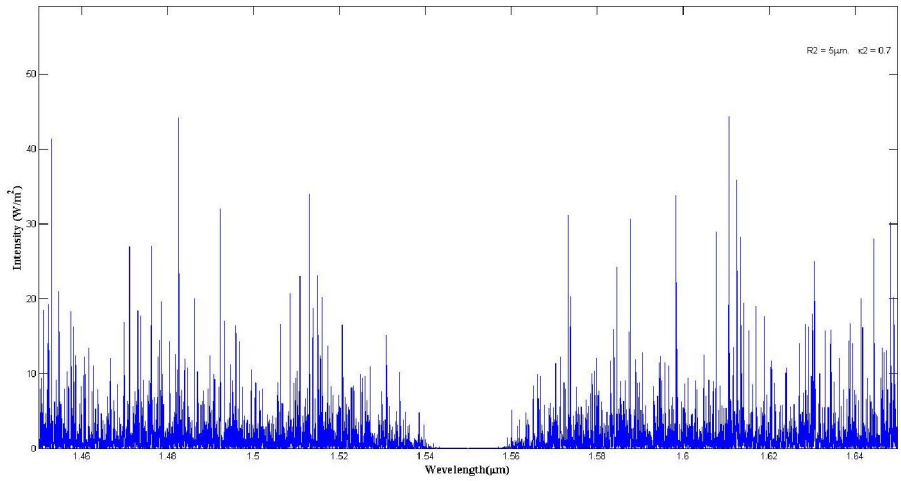

Figure 4.21 Output E_{R2} from ring R_2 .

This stage, the output power increase from 6W/m^2 to 45W/m^2.

Stage 3(R_d), the outputs of the first system by using the dark soliton pulse input, we get two outputs from the add/drop filter R_d , there are the E_{out} and E_d .

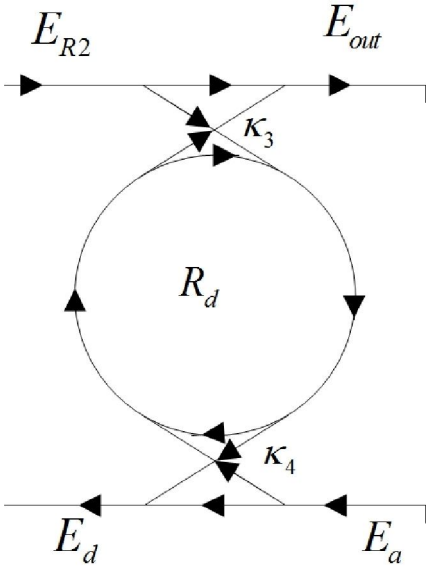

Figure 4.22 The add/drop filter R_d .

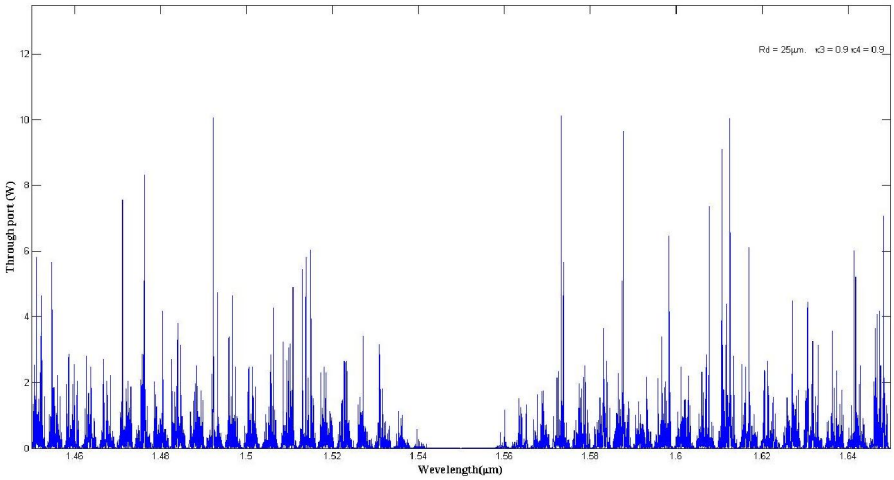

Figure 4.23 Output E_{out} at throughput port form add/drop filter R_d .

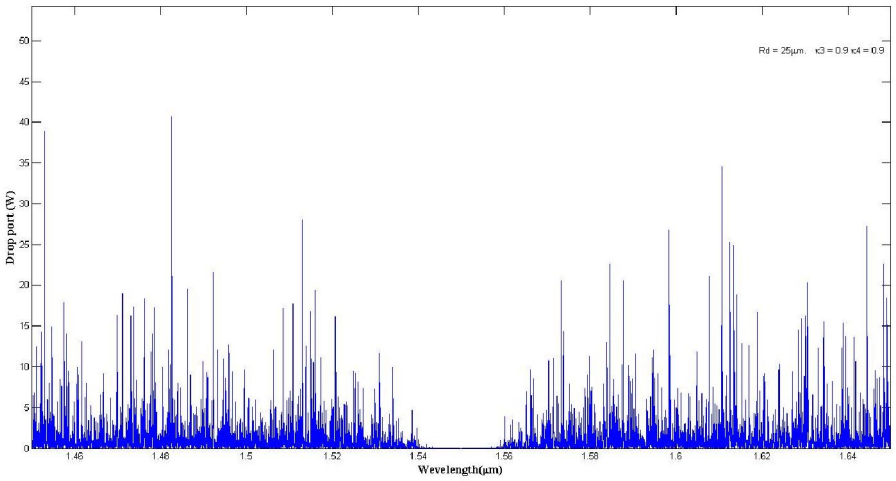

Figure 4.24 Output E_d at drop port form add/drop filter R_d.

In case of dark soliton pulse, the increasing powers same the Gaussian pulse and the bright soliton pulse. The throughput port has the output power at 10 W/m^2 and drop port can divide the excess power at 40 W/m^2.

We can see that after we input light pulses into the first system from three cases:

Case 1, the Gaussian pulse givens the bright soliton at throughput port, but not bright soliton at drop port.

Case 2, the bright soliton pulse givens the bright soliton at throughput and drop ports.

Case 3, the dark soliton pulse givens the bright soliton at throughput port, but not bright soliton at drop port.

Therefore, we get the bright solitons at throughput port from both light pulses, and the ring resonators can boost the power increased many fold.

4.2 The outputs of second system

For the second system, three type light pulse inputs are the bright soliton at throughput port of first system, and the parameters for the this system are ring radii, where R_1 = 16 μm, R_2 = 7 μm, R_3 = 5 μm, and R_d = 10 μm, linear refractive index, where n_0 = 3.34 (InGaAsP/InP), the nonlinear refractive index, where n_2 =2.2x10^{-17} m^2/W, effective mode core area, where A_{eff} = 0.50 μm^2 and 0.25 μm^2 for a microring resonator and add/drop filter, respectively, intensity attenuation coefficient α = 0.5 dB mm^{-1}, insertion loss γ = 0.1, coupling coefficient κ_1 =0.5, $\kappa_2 = \kappa_3$ =0.05, $\kappa_4 = \kappa_5$ =0.5, and the input light pulse are same first system.

Ring	R_1	R_2	R_3	R_d	n_0	n_2	A_{eff}	α	γ	κ_1	κ_2	κ_3	κ_4	κ_5
R_1	16	-	-	-	3.34	2.2x10^{-17}	0.5	0.5	0.1	0.5	-	-	-	-
R_2	-	7	-	-	3.34	2.2x10^{-17}	0.5	0.5	0.1	-	0.05	-	-	-
R_3	-	-	5	5	3.34	2.2x10^{-17}	0.5	0.5	0.1	-	-	0.05	-	-
R_d	-	-	-	10	3.34	2.2x10^{-17}	0.25	0.5	0.1	-	-	-	0.5	0.5

Table 4.2 the table of parameters for second system.

4.2.1 The output by using the Gaussian pulse as the input port

The Gaussian pulse with center wavelength (λ_0) at 1.55 μm, peak power at 1W/m^2 is input into the system as shown in Fig. 4.13.

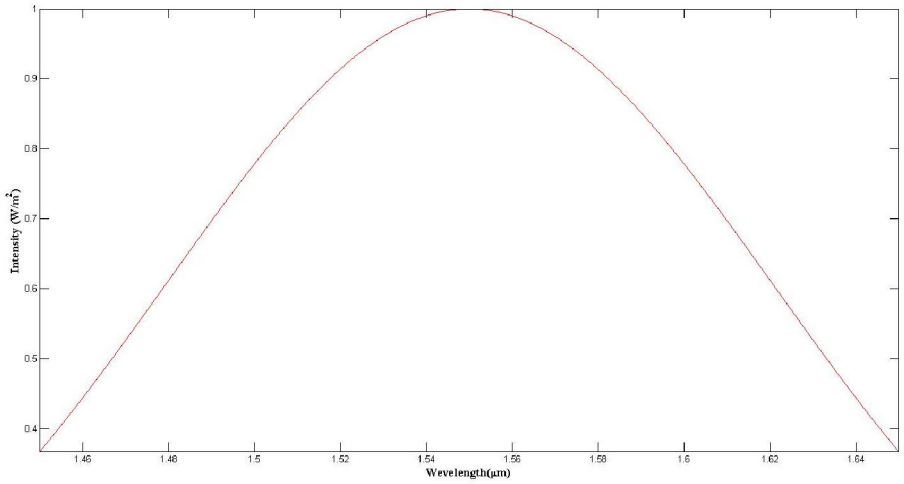

Figure 4.25 Gaussian pulse input E_{in} for second system.

The first stage (R_1), we get the E_{R1} from the first ring R_1.

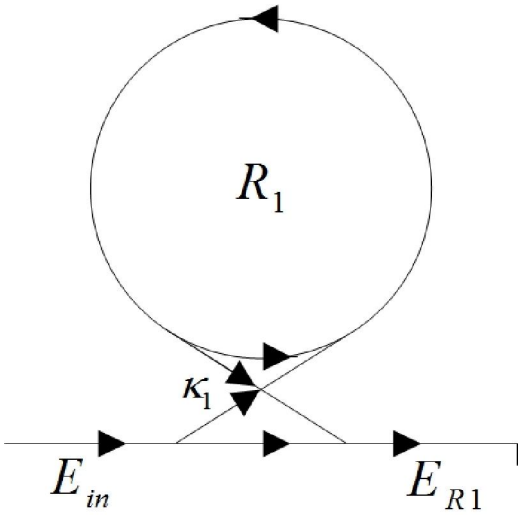

Figure 4.26 The ring R_1.

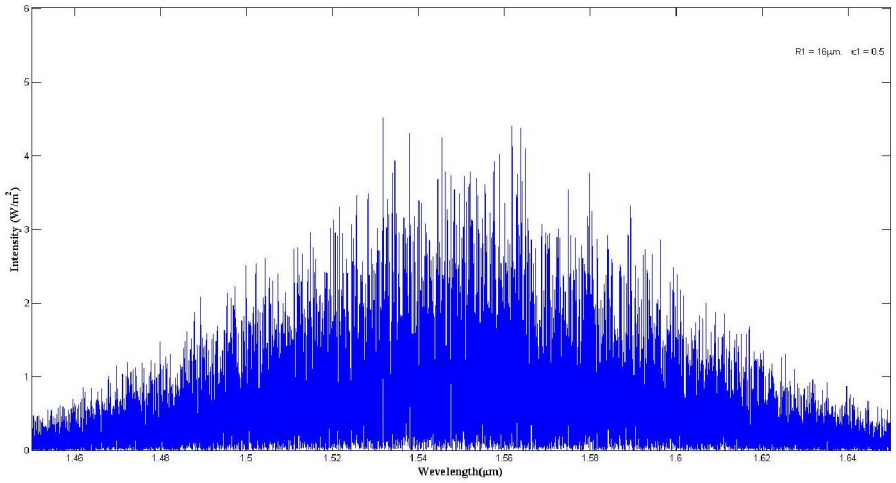

Figure 4.27 Output E_{R1} from ring R_1.

In this stage, the output power increase from 1W/m^2 to 5W/m^2.

Stage 2 (R_2), we get the E_{R2} from the second ring R_2 .

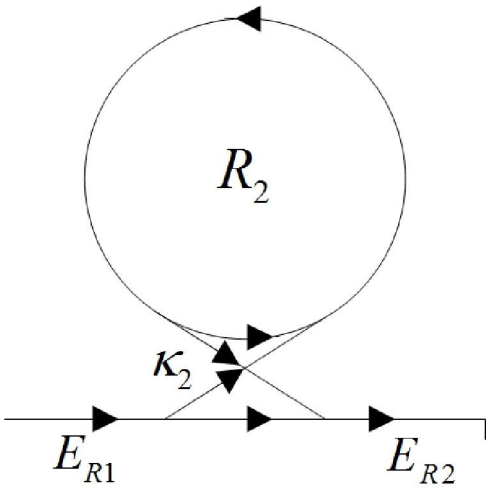

Figure 4.28 The ring R_2 .

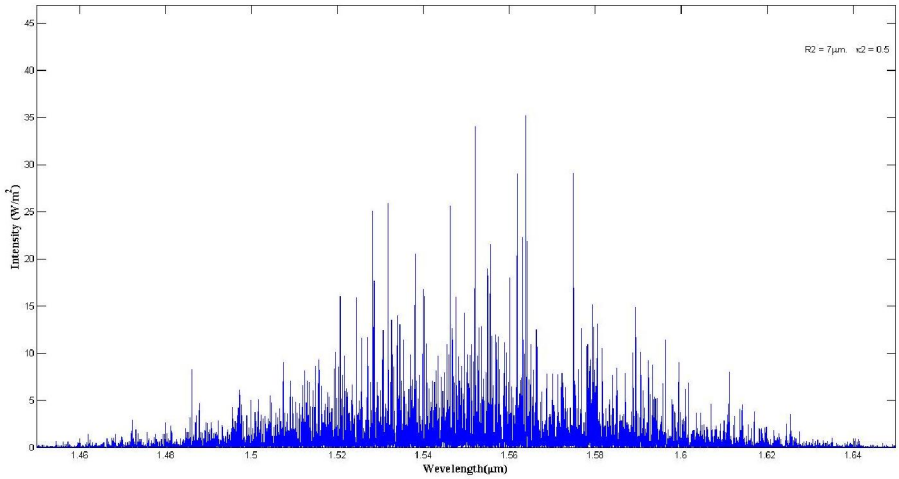

Figure 4.29 Output E_{R2} from ring R_2 .

This stage, the output power increase from 5W/m^2 to 35W/m^2.

Stage 3 (R_3), we get the E_{R3} from the second ring R_3 .

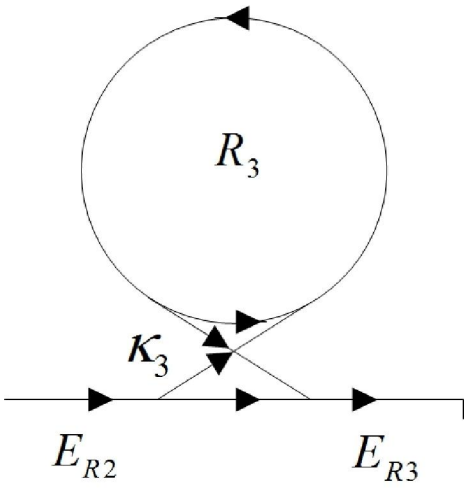

Figure 4.30 The ring R_3.

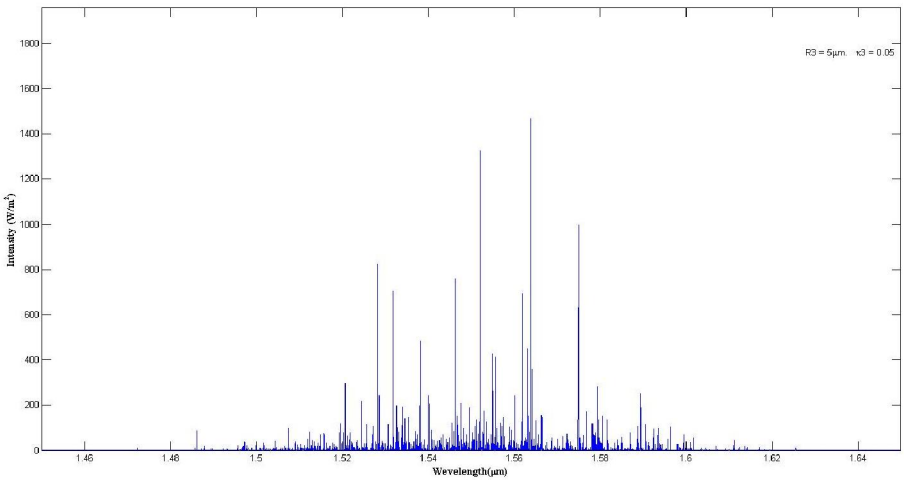

Figure 4.31 Output E_{R3} from ring R_3.

This stage, the output power increase from 35W/m^2 to 1500W/m^2.

Stage 4(R_d), the outputs of the first system by using the Gaussian pulse input, we get two outputs from the add/drop filter R_d, there are the E_{out} and E_d .

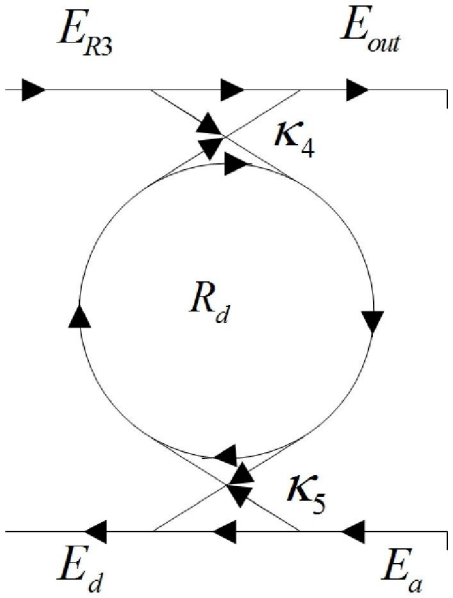

Figure 4.32 The add/drop filter R_d.

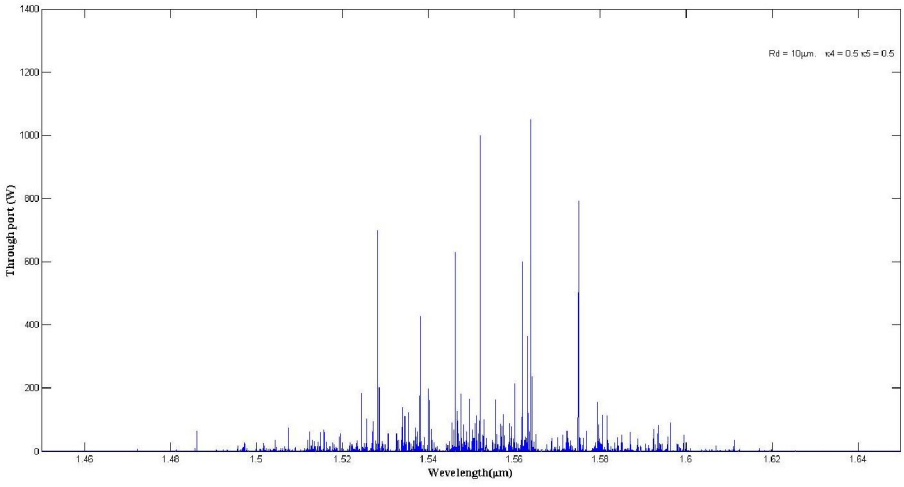

Figure 4.33 Output E_{out} at throughput port form add/drop filter R_d.

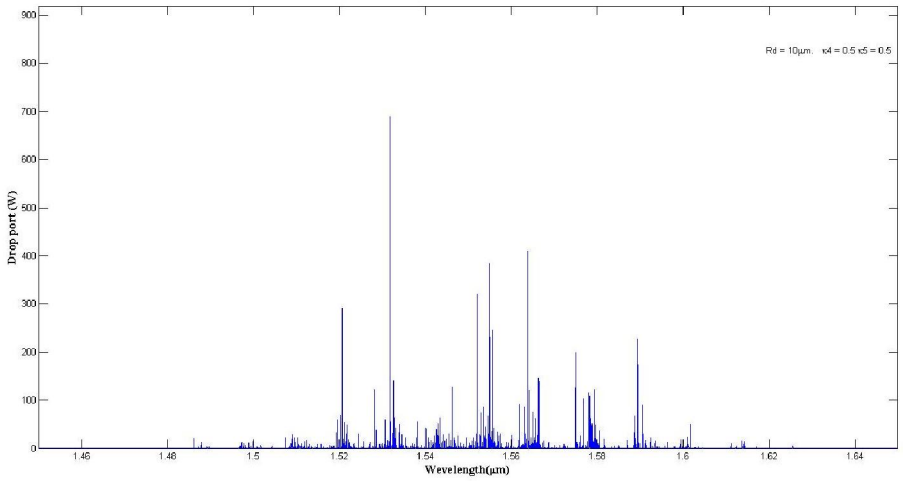

Figure 4.34 Output E_d at drop port form add/drop filter R_d.

In case of second system, we get the bright solitons at throughput port and drop port. The increasing of power similarly the first system, but it has very high power. The throughput port has the output power at 1100 W/m^2 and drop port can divide the excess power at 700 W/m^2.

4.2.2 The output by using the bright soliton pulse as the input port

The bright soliton pulse with center wavelength (λ_0) at 1.55 μm, peak power at 1W/m^2 is input into the system as shown in Fig. 4.18.

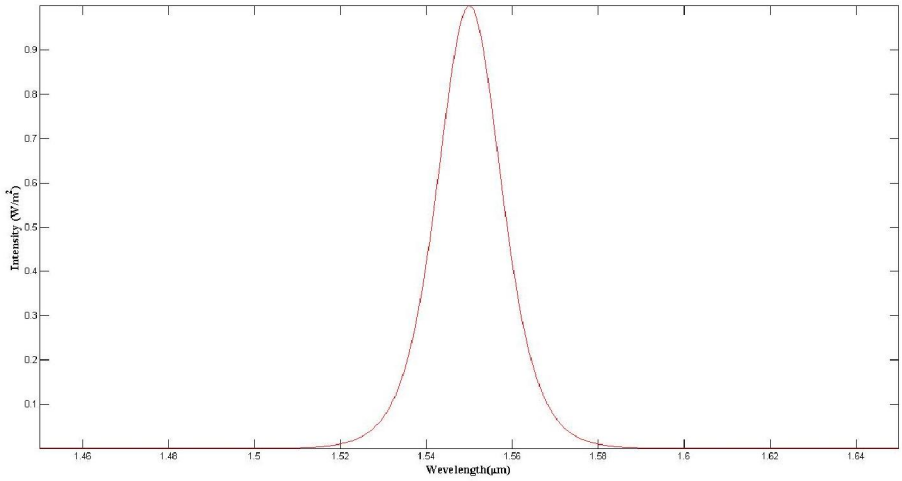

Figure 4.35 The bright soliton pulse input E_{in} for second system.

Stage 1 (R_1), we get the E_{R1} from the first ring R_1.

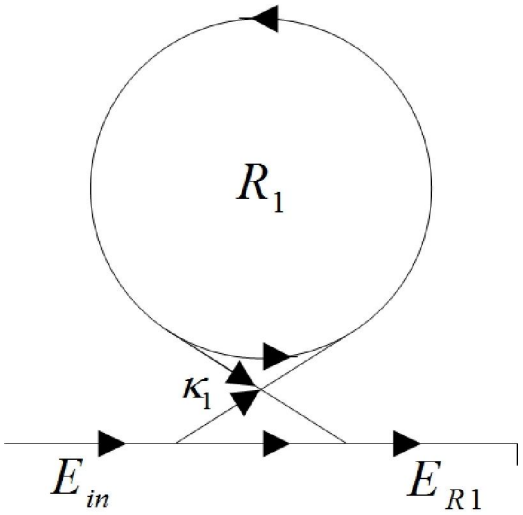

Figure 4.36 The ring R_1.

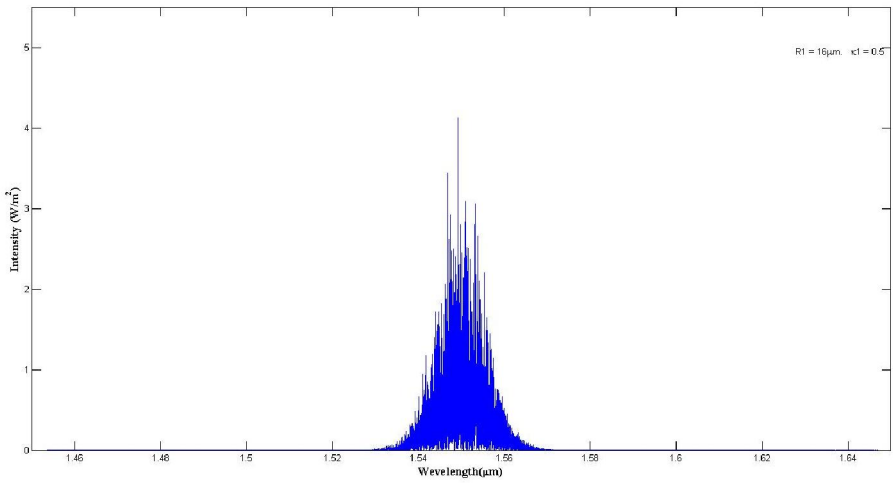

Figure 4.37 Output E_{R1} from ring R_1.

In this stage, the output power increase from 1W/m^2 to 4W/m^2.

Stage 2 (R_2), we get the E_{R2} from the second ring R_2 .

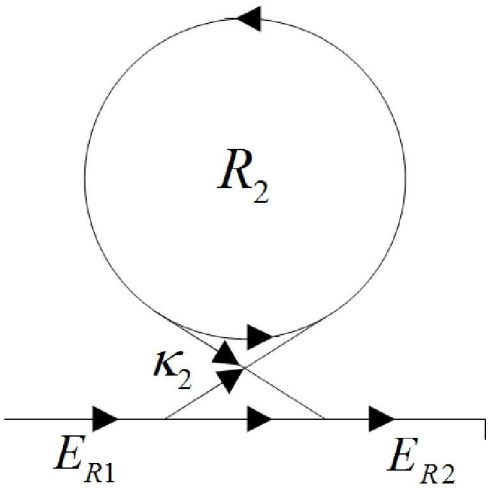

Figure 4.38 The ring R_2 .

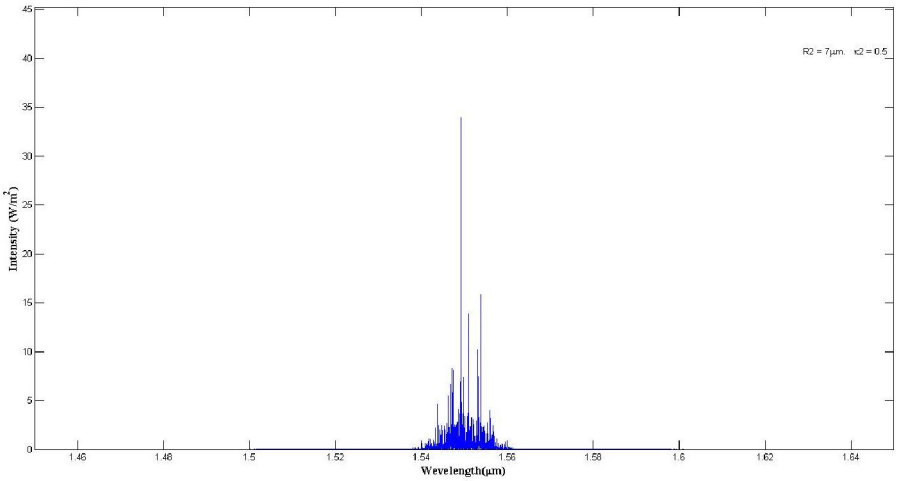

Figure 4.39 Output E_{R2} from ring R_2 .

This stage, the output power increase from 4W/m^2 to 35W/m^2.

Stage 3 (R_3), we get the E_{R3} from the second ring R_3 .

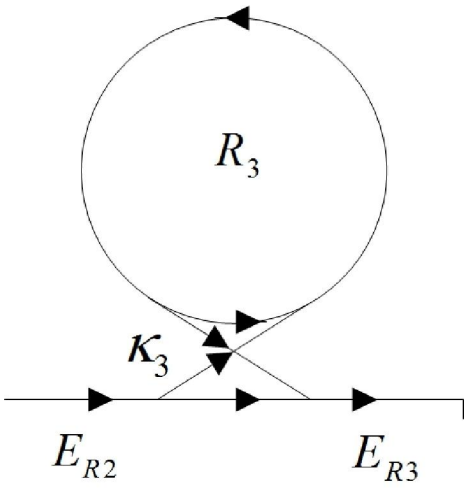

Figure 4.40 The ring R_3.

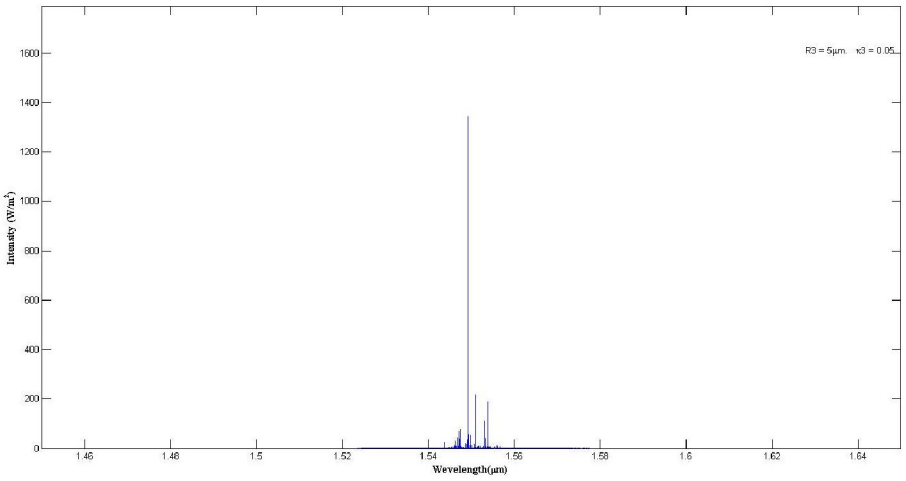

Figure 4.41 Output E_{R3} from ring R_3.

In this stage, the output power increase from 35W/m^2 to 1400W/m^2.

Stage 4(R_d), the outputs of the first system by using the bright soliton pulse input, we get two outputs from the add/drop filter R_d, there are the E_{out} and E_d .

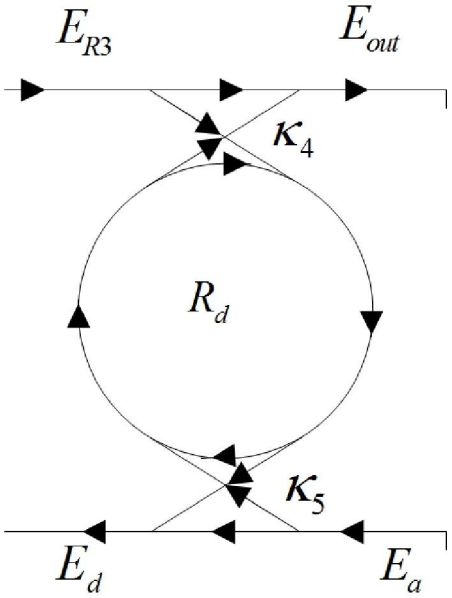

Figure 4.42 The add/drop filter R_d.

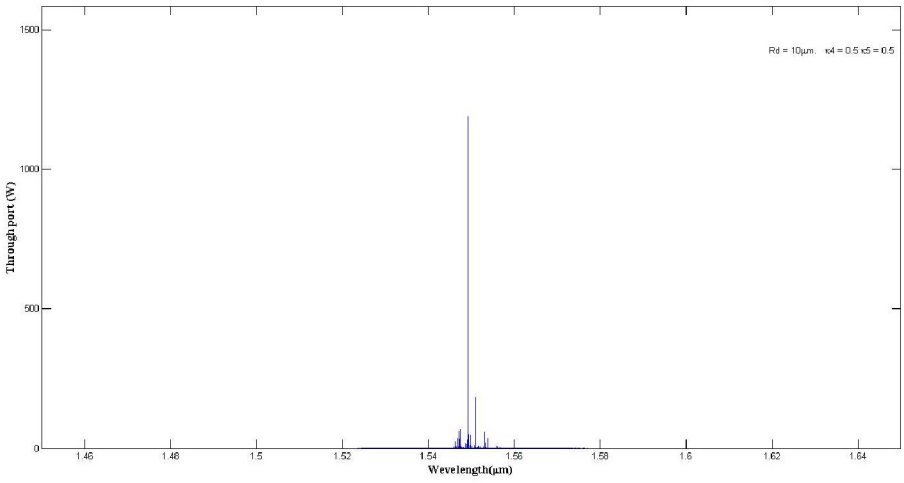

Figure 4.43 Output E_{out} at throughput port form add/drop filter R_d.

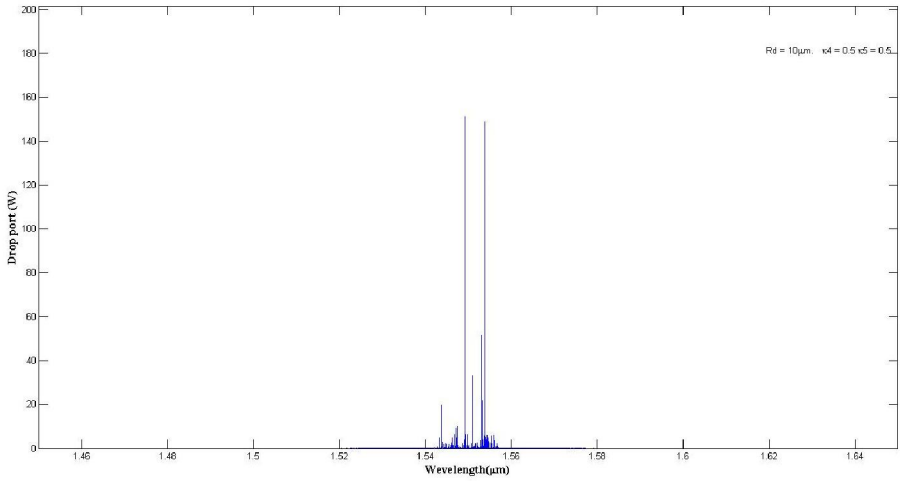

Figure 4.44 Output E_d at drop port form add/drop filter R_d.

In case of second system, we get the bright solitons at throughput port and drop port. The increasing of power similarly the Gaussian pulse. The throughput port has the output power at 1200 W/m^2 and drop port can divide the excess power at 150 W/m^2.

4.2.3 The output by using the dark soliton pulse as the input port

The dark soliton pulse with center wavelength (λ_0) at 1.55 μm, peak power at 1W/m^2 is input into the system as shown in Fig. 4.23.

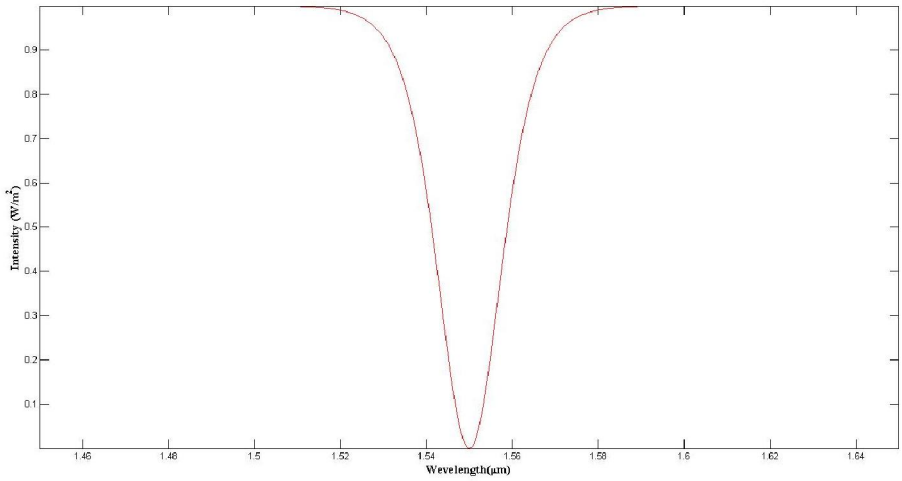

Figure 4.45 The dark soliton pulse input E_{in} for second system.

Stage 1 (R_1), we get the E_{R1} from the first ring R_1.

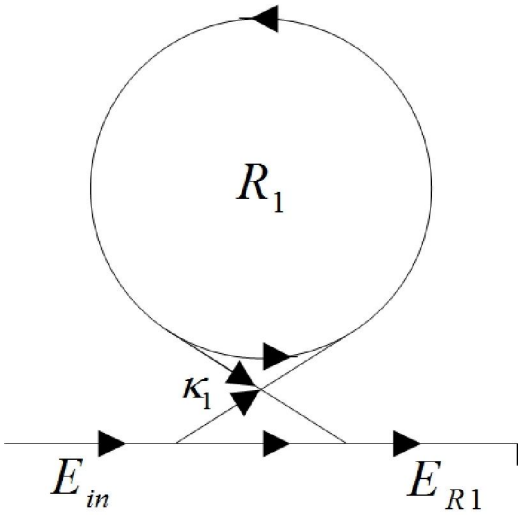

Figure 4.46 The ring R_1.

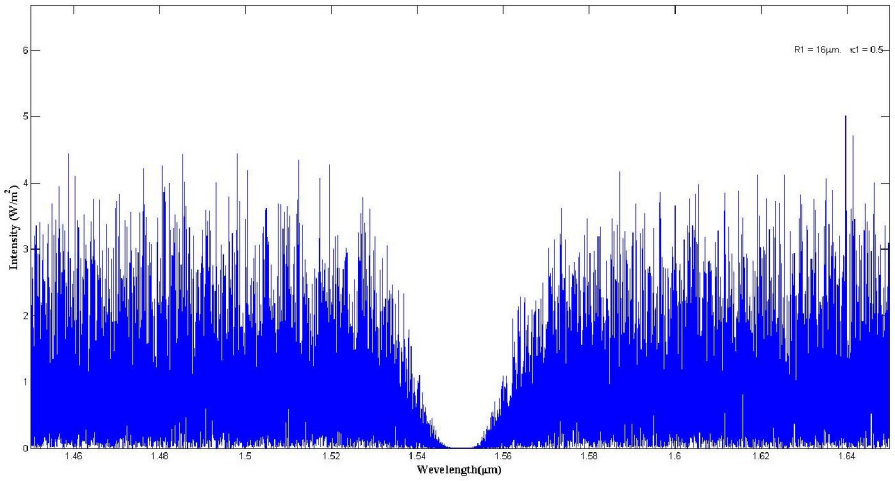

Figure 4.47 Output E_{R1} from ring R_1.

In this stage, the output power increase from 1W/m^2 to 5W/m^2.

Stage 2 (R_2), we get the E_{R2} from the second ring R_2 .

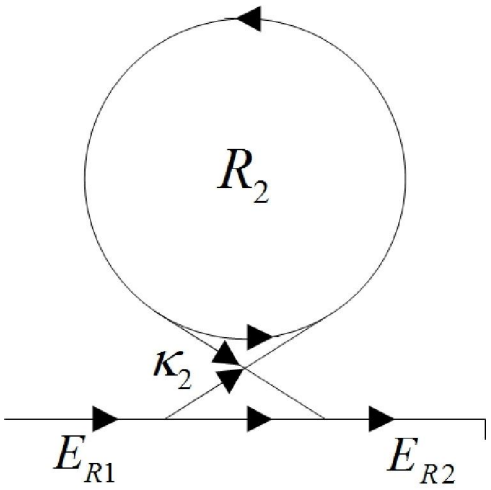

Figure 4.48 The ring R_2 .

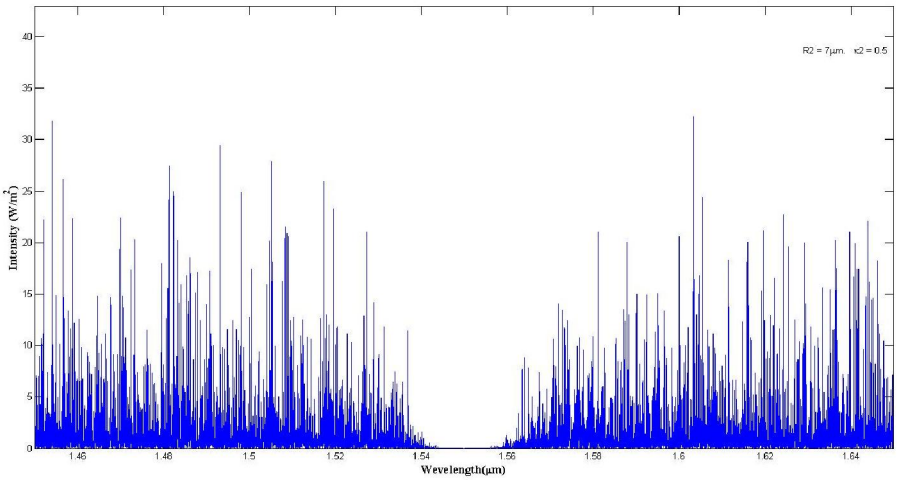

Figure 4.49 Output from ring R_2 .

In this stage, the output power increase from 5W/m^2 to 35W/m^2.

Stage 3 (R_3), we get the E_{R3} from the second ring R_3 .

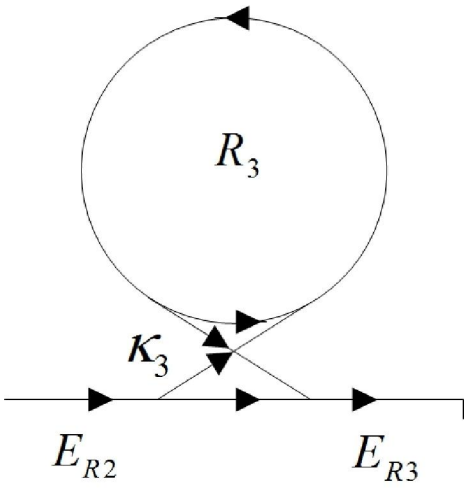

Figure 4.50 The ring R_3.

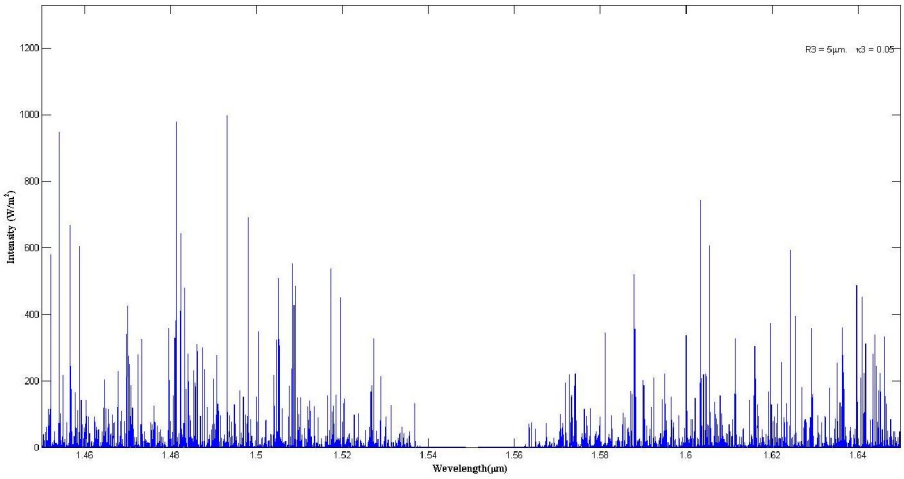

Figure 4.51 Output E_{R3} from ring R_3.

In this stage, the output power increase from 35W/m^2 to 1000W/m^2.

Stage 4(R_d), the outputs of the first system by using the dark soliton pulse input, we get two outputs from the add/drop filter R_d, there are the E_{out} and E_d .

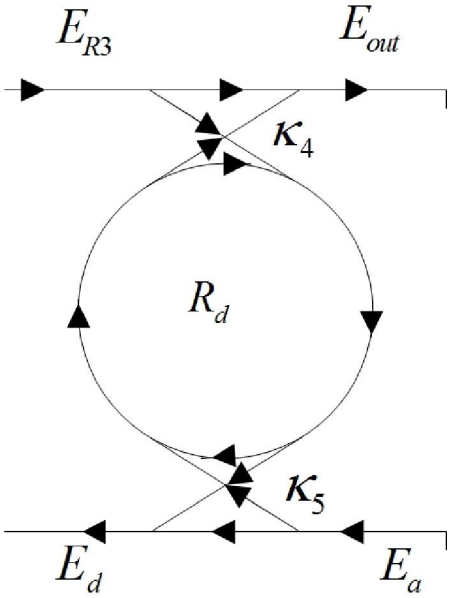

Figure 4.52 The add/drop filter R_d.

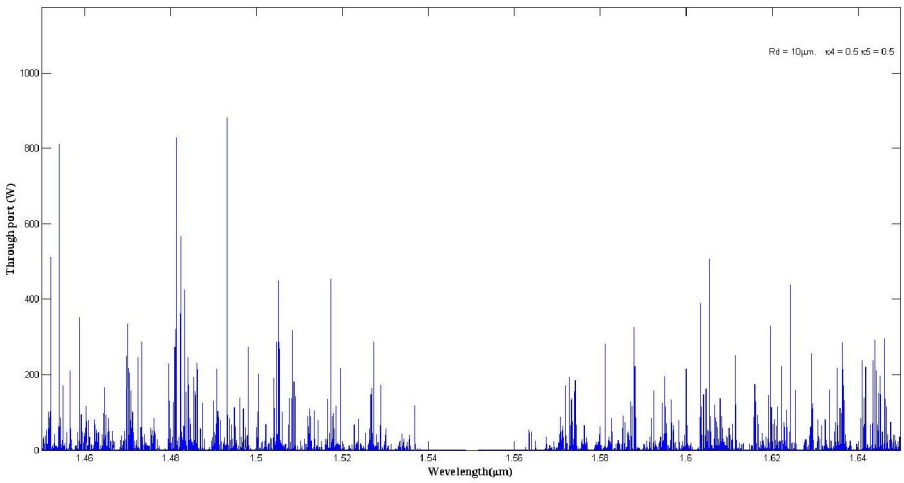

Figure 4.53 Output E_{out} at throughput port form add/drop filter R_d.

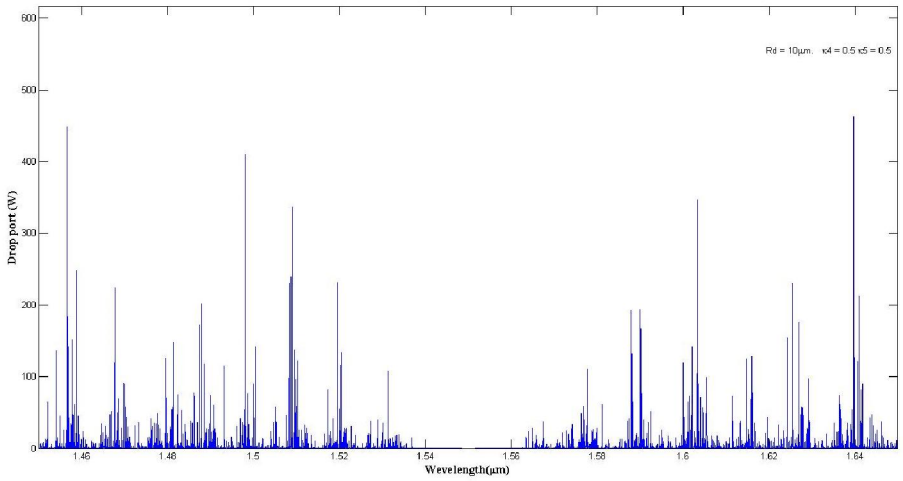

Figure 4.54 Output E_d at drop port form add/drop filter R_d.

In case of second system, we get the bright solitons at throughput port and drop port. The throughput port has the output power at 900 W/m^2 and drop port can divide the excess power at 500 W/m^2.

We can see that after we input light pulses into the second system from three cases:

Case 1, the Gaussian pulse givens the bright soliton at throughput and drop ports.

Case 2, the bright soliton pulse givens the bright soliton at throughput and drop ports.

Case 3, the dark soliton pulse givens the bright soliton at throughput and drop ports.

Therefore, we get the bright solitons at throughput and drop ports from both light pulses, and we have the interesting result, that is the bright solitons at throughput port from the Gaussian pulse input, and the ring resonators can boost the power increased many fold.

Chapter V

Conclusions and Suggestions

5.1 Conclusions

This thesis studies the effect of the light pulse passing through ring resonator systems. The inputs are light pulses of three forms: the Gaussian pulse, the dark soliton and the bright soliton. The simulation shows that light pulses gain more power when passing through the system. The outputs are in the form of bright solitons, available at the throughput port and/or the drop port, depending on the configuration of the ring resonator used.

The power of the output of the first system is tenfold that of the input while the power of the output of the second system is boosted thousand fold.

5.2 Suggestions

This encounter allows the invention of bright soliton generators using laser pulse (Gaussian pulse), which is available at low cost.

The bright solitons outputs can distribute by the mutiphotons trapping within the potential well.

The ring resonator system can boost the power of light pulses and therefore, it can be used to make a repeater.

References

[1] Venghaus, H., Editor. 2006. **Wavelength Filters in Fibre Optics.** Berlin : Springer.

[2] Agarwal, G.P., 2007. **Nonlinear Fiber Optics.** 4th ed. New York : Academic Press.

[3] Dinh, 2015. P.M., **Study Guide for An Introduction to Cluster Science.** 1st ed. United States : Cram101.

[4] Greivenkamp, J.E., 2004. **Field Guide to Geometrical Optics.** Washington : SPIE.

[5] R. Paschotta, 2015. **Optical intensity**. [Online]. Available : http://www.rp-photonics.com/optical_intensity.html.

[6] Vardeny, Z.V., 2002. **"Telecommunications: A boost for fibre optics".** Nature 416 : 489–491.

[7] Pozar, D.M., 2011. **Microwave Engineering.** 4th ed. The United States of America : John Wiley & Sons.

[8] microwaves101.com, 2015. **"Phase constant versus wavenumber".** [Online]. Available : http://www.microwaves101.com/encyclopedias/propagation-constant.

[9] Alegria, C.F.G., 2001. **"All-Fibre Devices for WDM Optical Communications."** Ph.D. Thesis of University of Southampton.

[10] Rüdiger, P., 2008. **Encyclopedia of Laser Physics and Technology.** Berlin : Wiley.

[11] Amiri, S.I. and Afroozeh A., 2015. **Ring Resonator Systems to Perform Optical Communication Enhancement Using Soliton.** New York : Springer.

[12] Eugene, H., 2002. **Optics.** 4th ed. The United States of America : Addison-Wesley.

[13] Xiao, Y.F., Min, B., Jiang, X., Dong, C.H., and Yang, L., 2008. **"Coupling Whispering-Gallery-Mode Microcavities With Modal Coupling Mechanism."** IEEE Journal of Quantum Electronics. 44(11) : 1065-1070.

[14] Rabus, D.G. **"Realization of Optical Filters using Ring Resonators with integrated Semiconductor Optical Amplifiers in GaInAsP / InP."** Ph.D. Thesis of University Berlin.

Appendix

Lists of Publications

[1] Yupapin, P.P., Vanishkorn, B. 2011. **"Mathematical simulation of light pulse propagating within a microring resonator system and applications."** Applied Mathematical Modelling. 35 : 1729-1738.

[2] Vanishkorn, B. Srinuanjan, K. Yupapin, P.P. 2011. **"Multiphotons trapping instability using fiber Bragg's grating potential perturbation for multiquantum bits encoding."** Optik. 122 : 506-509.

Applied Mathematical Modelling 35 (2011) 1729–1738

Contents lists available at ScienceDirect

Applied Mathematical Modelling

journal homepage: www.elsevier.com/locate/apm

Mathematical simulation of light pulse propagating within a microring resonator system and applications

P.P. Yupapin *, B. Vanishkorn

Nanoscale Science and Engineering Research Alliance, Advanced Research Center for Photonics Faculty of Science, King Mongkut's Institute of Technology Ladkrabang, Bangkok 10520, Thailand

ARTICLE INFO

Article history:
Received 26 July 2009
Received in revised form 21 September 2010
Accepted 4 October 2010
Available online 16 October 2010

Keywords:
Engineering mathematics
Mathematical modeling
Computational physics
Mathematical simulation

ABSTRACT

This paper presents the very fascinating simulation results of light pulse traveling within a ring resonator system that have shown the unexpected results with various applications. The design system consists of a nonlinear microring/nanoring resonator system incorporating an add/drop filter. The proposed fabricated material used is InGaAsP/InP, which can provide the required output behaviors. Three different forms of input light pulses are Gaussian pulse, dark and bright soliton, whereas the suitable simulation parameters are input power, pulse width, ring radii and the material refractive indices. Three different forms of the results have been interpreted, whereas the dominants behaviors are such as Gaussian soliton, multisoliton and tunable dark soliton are described, and the potential applications for new laser sources, new communication bands and dynamic optical tweezers have been discussed.

1. Introduction

A Gaussian pulse has been recognized in the form of a laser pulse that can be used in both theoretical and experimental investigation in many subjects. However, in some ways, the limit of laser power cause a problem, especially, when the high output power or long distance link is required. Optical soliton becomes a powerful tool that can overcome such a problem, i.e. for high power laser source. Furthermore, the non-dispersion of soliton in medium is the other advantage. Optical solitons can naturally be divided into classes of dark and bright solitons, whereas a dark soliton exhibits an interesting and remarkable behavior, when it is transmitted into an optical transmission system. It has the advantage of the signal detection difficulty, when the ambiguity of signal detection becomes a problem for the un-wanted users. In principle, the soliton generations and their behaviors in media are well analyzed and described by Agarwal [1]. Many earlier theoretical and experimental works on soliton applications can be found in the soliton application book by Hasegawa [2]. However, to make such a tool more useful, the problems of soliton–soliton interactions [3], collision [4], rectification [5], and dispersion management [6–8] must be solved and addressed. Therefore, in this work, we are looking for a powerful laser source with broad spectrum that can be used in many applications.

Recently, several research works have shown that use of dark and bright soliton in various applications can be realized [9–14], where one of them has shown that the secured signals in the communication link can be retrieved by using a suitable an add/drop filter that is connected into the transmission line. The other promising application of a dark soliton signal [15] is for the large guard band of two different frequencies which can be achieved by using a dark soliton generation scheme and trapping a dark soliton pulse within a nanoring resonator [1]. Furthermore, the dark soliton pulse shows a more stable

* Corresponding author. Tel.: +66 2 3264342; fax: +66 2 3264354.
E-mail address: kypreech@kmitl.ac.th (P.P. Yupapin).

0307-904X/$ - see front matter © 2010 Elsevier Inc. All rights reserved.
doi:10.1016/j.apm.2010.10.005

behavior than the bright solitons with respect to the perturbations such as amplifier noise, fiber losses, and intra-pulse stimulated Raman scattering [16]. It is found that the dark soliton pulses propagation in a lossy fiber, spreads in time at approximately half the rate of bright solitons. The dark solitons trapped in add/drop system is realized [17]. In this paper, the use of three forms of laser pulses, i.e. Gaussian soliton, dark and bright soliton propagating within the proposed ring resonator systems is investigated and described. The use of suitable simulation parameters based on the realistic device is discussed. The potential application for new laser sources, new communication bands and dynamic optical tweezers is also discussed.

2. Theory and principle

2.1. Gaussian pulse

Light from a monochromatic light source is launched into a ring resonator with constant light field amplitude (E_0) and random phase modulation as shown in Fig. 1, which is the combination of terms in attenuation (α) and phase (φ_0) constants, which results in temporal coherence degradation. Hence, the time dependent input light field (E_{in}), without pumping term, can be expressed as [18]

$$E_{in}(t) = E_0 e^{-\alpha L + j\phi_0(t)}, \tag{1}$$

where L is a propagation distance(waveguide length).

We assume that the nonlinearity of the optical ring resonator is of the Kerr-type, i.e., the refractive index is given by

$$n = n_0 + n_2 I = n_0 + \left(\frac{n_2}{A_{eff}}\right)P, \tag{2}$$

where n_0 and n_2 are the linear and nonlinear refractive indexes, respectively. I and P are the optical intensity and optical power, respectively. The effective mode core area of the device is given by A_{eff}. For the microring and nanoring resonators, the effective mode core areas range from 0.10 to 0.50 μm^2 [19,20].

When a Gaussian pulse is input and propagated within a fiber ring resonator, the resonant output is formed, thus, the normalized output of the light field is the ratio between the output and input fields (E_{out} and E_{in}) in each roundtrip, which can be expressed as [21]

$$\frac{|E_{out}(t)|^2}{|E_{in}(t)|} = (1-\gamma)\left[1 - \frac{(1-(1-\gamma)x^2)\kappa}{(1-x\sqrt{1-\gamma}\sqrt{1-\kappa})^2 + 4x\sqrt{1-\gamma}\sqrt{1-\kappa}\sin^2(\frac{\phi}{2})}\right]. \tag{3}$$

Eq. (3) indicates that a ring resonator in the particular case is very similar to a Fabry–Perot cavity, which has an input and output mirror with a field reflectivity, $(1-\kappa)$, and a fully reflecting mirror. k is the coupling coefficient, and ($x = \exp(-\alpha L/2)$ represents a roundtrip loss coefficient, $\varphi_0 = kLn_0$ and $\phi_{NL} = kL\left(\frac{n_2}{A_{eff}}\right)P$ are the linear and nonlinear phase shifts, $k = 2\pi/\lambda$ is the wave propagation number in a vacuum. Where L and α are a waveguide length and linear absorption coefficient, respectively. In this work, the iterative method is introduced to obtain the results as shown in Eq. (3), similarly, when the output field is connected and input into the other ring resonators.

The input optical field as shown in Eq. (1), i.e. a Gaussian pulse, is input into a nonlinear microring resonator. By using the appropriate parameters, the chaotic signal is obtained by using Eq. (3). To retrieve the signals from the chaotic noise, we propose to use the add/drop device with the appropriate parameters. This is given in details as followings. The optical outputs of a ring resonator add/drop filter can be given by the Eqs. (4) and (5).

$$\frac{|E_t|^2}{|E_{in}|} = \frac{(1-\kappa_1) - 2\sqrt{1-\kappa_1}\cdot\sqrt{1-\kappa_2}e^{-\frac{\alpha L}{2}}\cos(k_n L) + (1-\kappa_2)e^{-\alpha L}}{1 + (1-\kappa_1)(1-\kappa_2)e^{-\alpha L} - 2\sqrt{1-\kappa_1}\cdot\sqrt{1-\kappa_2}e^{-\frac{\alpha L}{2}}\cos(k_n L)}, \tag{4}$$

and

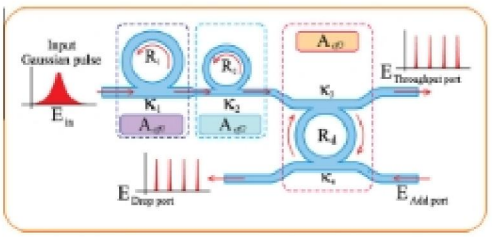

Fig. 1. A schematic of a Gaussian soliton generation system, where R_i: ring radii, κ_i: coupling coefficients, R_4: an add/drop ring radius, A_{eff}: effective areas.

$$\left|\frac{E_d}{E_{in}}\right|^2 = \frac{\kappa_1\kappa_2 e^{-\frac{\alpha L}{2}}}{1+(1-\kappa_1)(1-\kappa_2)e^{-\alpha L} - 2\sqrt{1-\kappa_1}\cdot\sqrt{1-\kappa_2}e^{-\frac{\alpha L}{2}}\cos(k_o L)}, \tag{5}$$

where E_t and E_d represents the optical fields of the throughput and drop ports respectively. The transmitted output can be controlled and obtained by choosing the suitable coupling ratio of the ring resonator, which is well derived and described by reference [21]. Where $\beta = kn_{eff}$ represents the propagation constant, n_{eff} is the effective refractive index of the waveguide, and the circumference of the ring is $L = 2\pi R$, here R is the radius of the ring. The chaotic noise cancellation can be managed by using the specific parameters of the add/drop device, which the required signals at the specific wavelength band can be filtered and retrieved. K_1 and K_2 are coupling coefficient of add/drop filters, $k_o = 2\pi/\lambda$ is the wave propagation number for in a vacuum, and the waveguide (ring resonator) loss is $\alpha = 0.5$ dB mm^{-1}. The fractional coupler intensity loss is $\gamma = 0.1$. In the case of add/drop device, the nonlinear refractive index is neglected.

2.2. Soliton

Bright and dark soliton pulses are introduced into the multistage nanoring resonators as shown in Fig. 2, the input optical field (E_{in}) of the bright and dark soliton pulses input are given by an Eq. (6) and (7)[1], respectively:

$$E_{in}(t) = A\,\mathrm{sech}\left[\frac{T}{T_0}\right]\exp\left[\left(\frac{z}{2L_D}\right) - i\omega_0 t\right], \tag{6}$$

and

$$E_{in}(t) = A\tanh\left[\frac{T}{T_0}\right]\exp\left[\left(\frac{z}{2L_D}\right) - i\omega_0 t\right], \tag{7}$$

where A and z are the optical field amplitude and propagation distance, respectively. T is a soliton pulse propagation time in a frame moving at the group velocity, $T = t - \beta_1 z$, where β_1 and β_2 are the coefficients of the linear and second-order terms of Taylor expansion of the propagation constant. $LD = T_0^2/|\beta_2|$ is the dispersion length of the soliton pulse. T_0 in equation is a soliton pulse propagation time at initial input (or soliton pulse width), where t is the soliton phase shift time, and the frequency shift of the soliton is ω_0. This solution describes a pulse that keeps its temporal width invariance as it propagates, and thus is called a temporal soliton. When a soliton peak intensity $|\beta_2/\Gamma T_0^2|$ is given, then T_0 is known. For the soliton pulse in the microring device, a balance should be achieved between the dispersion length (L_D) and the nonlinear length ($L_{NL} = 1/\Gamma\varphi_{NL}$), where $\Gamma = n_2 k_o$, is the length scale over which dispersive or nonlinear effects makes the beam become wider or narrower. For a soliton pulse, there is a balance between dispersion and nonlinear lengths, hence $L_D = L_{NL}$. Similarly, the output soliton of the system in Fig. 2 can be calculated by using Gaussian equations as given in the above case.

3. Results

3.1. Gaussian pulse

From Fig. 1, in principle, light pulse is sliced to be the discrete signal and amplified within the first ring, where more signal amplification can be obtained by using the smaller ring device (second ring). Finally, the required signals can be obtained via a drop port of the add/drop filter. In operation, an optical field in the form of Gaussian pulse from a laser source at the specified center wavelength is input into the system. From Fig. 3, the Gaussian pulse with center wavelength (λ_0) at 0.40 μm, pulse width (full width at half maximum, FWHM) of 20 ns, peak power at 2 W is input into the system as shown in Fig. 3(a). The large bandwidth signals can be seen within the first microring device, and shown in Fig. 3(b). The suitable ring

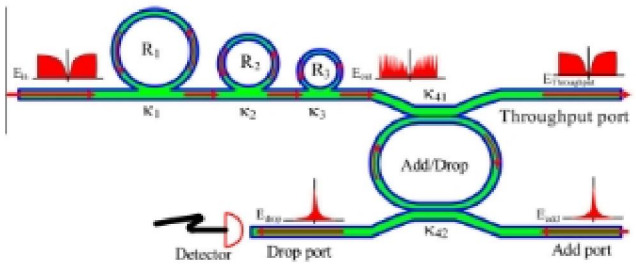

Fig. 2. Schematic of a dark–bright soliton conversion system, where R_i is the ring radii, κ_i is the coupling coefficient, and κ_{41} and κ_{42} are the add/drop coupling coefficients.

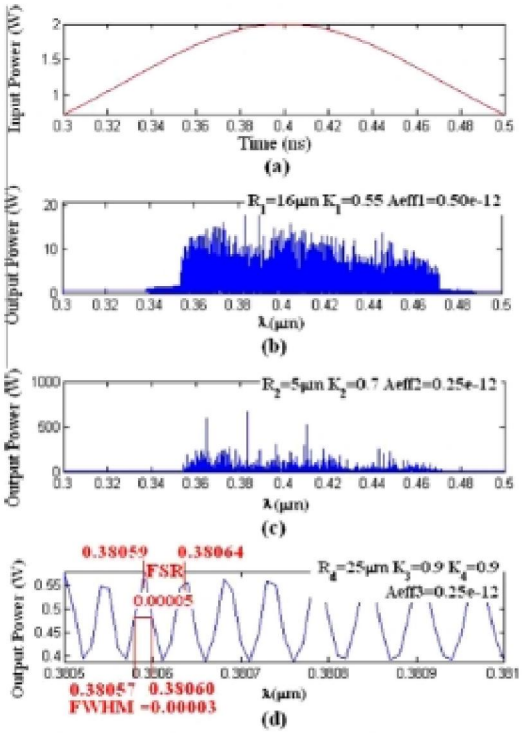

Fig. 3. Result of the spatial pulses with center wavelength at 0.40 μm, where (a) the Gaussian pulse, (b) large bandwidth signals, (c) large amplified signals, (d) filtering and amplifying signals from the drop port.

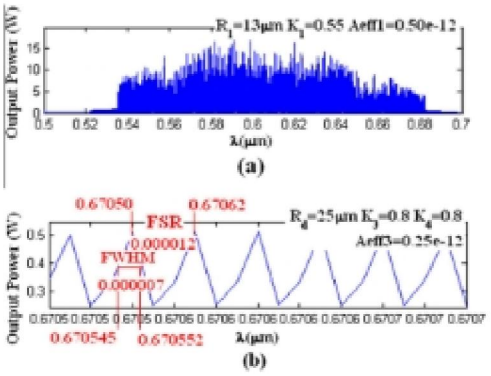

Fig. 4. Result of the spatial pulses with center wavelength at 0.60 μm, where (a) large bandwidth signals, (b) filtering and amplifying signals from the drop port.

parameters are used, for instance, ring radii R_1 = 16.0 μm, R_2 = 5.0 μm, and R_d = 25.0 μm. In order to make the system associate with the practical device [19,20], the selected parameters of the system are fixed to n_0 = 3.34 (InGaAsP/InP), A_{eff} = 0.50 μm^2 and 0.25 μm^2 f or a microring and add/drop ring resonator, respectively, α = 0.5 dB mm^{-1}, γ = 0.1. In this investigation, the coupling coefficient (kappa, κ) of the microring resonator is ranged from 0.55 to 0.90. The nonlinear refractive index of the microring used is $n_2 = 2.2 \times 10^{-17}$ m^2/W. In this case, the attenuation of light propagates within the system (i.e. wave guided) used is 0.5 dB mm^{-1}. After light is input into the system, the Gaussian pulse is chopped (sliced) into a smaller signal spreading over the spectrum due to the nonlinear effects [22], which is shown in Fig. 3(a). The large bandwidth signal is generated within the first ring device. In applications, the specific input or out wavelengths can be used and generated. For instance, the different center wavelengths of the input pulse can be ranged from 0.40 to 1.5 μm as shown in Figs. 3–8, where the suitable parameters are used and shown in the figures.

3.2. Dark soliton

In operation, a dark soliton pulse with 50-ns pulse width with the maximum power of 0.65 W is input into the dark-bright soliton conversion system as shown in Fig. 2. The suitable ring parameters are ring radii, where R_1 = 10.0 μm, R_2 = 7.0 μm, and R_3 = 5.0 μm. In order to make the system associate with the practical device [19,20] the selected parameters of the system are fixed to λ_0 = 1.50 μm, n_0 = 3.34 (InGaAsP/InP). The effective core areas are A_{eff} = 0.50, 0.25, and 0.10 μm^2 for

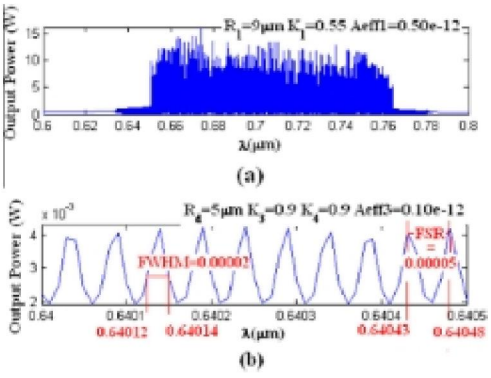

Fig. 5. Result of the spatial pulses with center wavelength at 0.70 μm, where (a) large bandwidth signals, (b) filtering and amplifying signals from the drop port.

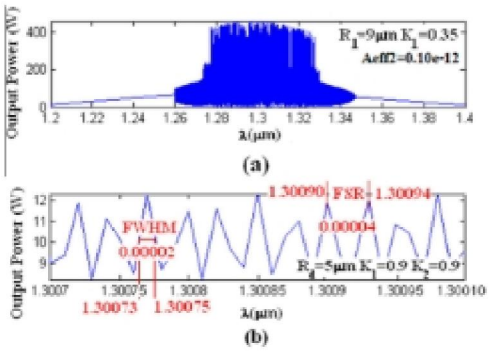

Fig. 6. Result of the spatial pulses with center wavelength at 1.30 μm, where (a) large bandwidth signals, (b) filtering and amplifying signals from the drop port.

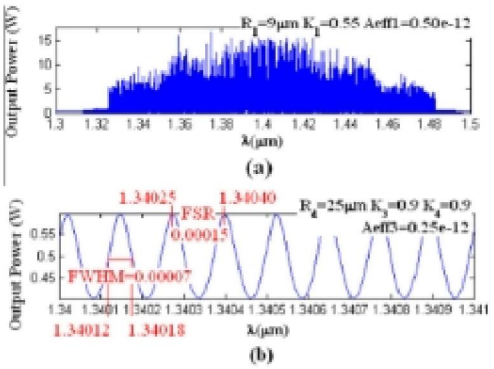

Fig. 7. Result of the spatial pulses with center wavelength at 1.40 μm, where (a) large bandwidth signals, (b) filtering and amplifying signals from the drop port.

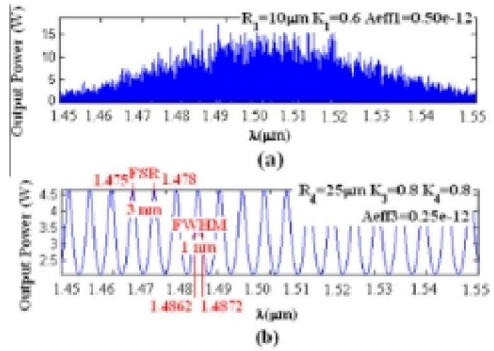

Fig. 8. Results of the spatial pulses with center wavelength at 1.50 μm, where (a) large bandwidth signals, (b) filtering and amplifying signals from the drop port.

a microring resonator (MRR) and nanoring resonator (NRR), respectively. The waveguide and coupling loses are $\alpha = 0.5$ dB mm^{-1} and $\gamma = 0.1$, respectively, and the coupling coefficients κ_i of the MRR are ranged from 0.05 to 0.90. However, more parameters are used as shown in Fig. 2. The nonlinear refractive index is $n_2 = 2.2 \times 10^{-13}$ m^2/W. In this case, the waveguide loss used is 0.5 dB mm^{-1}. The input dark soliton pulse is chopped (sliced) into the smaller output signals of the filtering signals within the rings R_2 and R_3. We find that the output signals from R_3 are smaller than from R_1, which is more difficult to detect when it is used in the link. In fact, the multistage ring system is proposed due to the different core effective areas of the rings in the system, where the effective areas can be transferred from 0.50 to 0.10 μm^2 with some losses. The soliton signals in R_3 is entered in the add/drop filter, where the dark-bright soliton conversion can be performed by using Eqs. (6) and (7). Results obtained when a dark soliton pulse is input into a MRR and NRR system as shown in Fig. 9. The add/drop filter is formed by two couplers and a ring radius (R_4) of 10 μm, the coupling constants (κ_{41} and κ_{42}) are the same values (0.50). When the add/drop filter is connected to the third ring (R_3), the dark-bright soliton conversion can be seen. The bright and dark solitons are detected by the through (throughput) and drop ports as shown in Fig. 9(d) and (e), respectively.

3.3. Bright soliton

The large bandwidth signal within the micro ring device can be generated by using a common soliton pulse input into the nonlinear micro ring resonator. This means that the broad spectrum of light can be generated after the soliton pulse is input into the ring resonator system. The schematic diagram of the proposed system is as shown in Fig. 12. A soliton pulse with

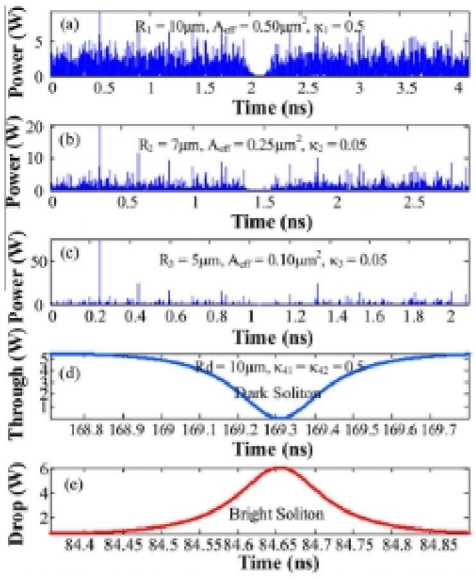

Fig. 9. Results of the soliton signals within the ring resonator system, where (a) in ring R1, (b) in ring R2, (c)–(d) in ring R3, and (d)–(e) dark, bright solitons conversion at the add/drop filter. The input dark soliton power is 2 W.

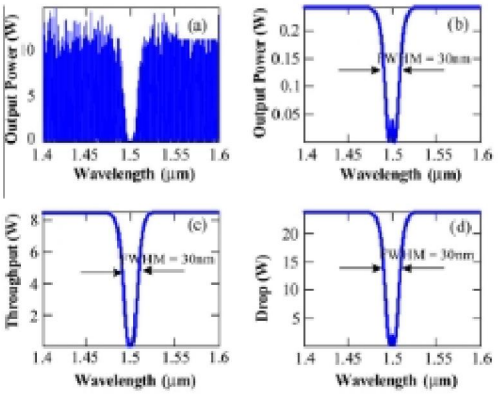

Fig. 10. Shows the dynamic dark soliton (optical tweezers) within the add/drop filter, when the bright soliton is input into the add port with the center wavelength $\lambda_0 = 1.5$ μm: (a) add/drop signals, (b) dark-bright soliton collision, (c) optical tweezers at throughput port, and (d) optical tweezers at drop port.

50 ns pulse width, peak power at 2 W is input into the system. The suitable ring parameters are used, for instance, ring radii $R_1 = 15.0$ μm, $R_2 = 10.0$ μm, $R_3 = R_s = 5.0$ μm and $R_5 = R_d = 20.0$ μm. In order to make the system associate with the practical device [19,20], the selected parameters of the system are fixed to $\lambda_0 = 1.55$ μm, $n_0 = 3.34$ (InGaAsP/InP), $A_{eff} = 0.50$, 0.25 μm^2 and 0.10 μm^2 for a micro ring and nanoring resonator, respectively, $\alpha = 0.5$ dB mm^{-1}, $\gamma = 0.1$. The coupling coefficient (kappa, κ) of the micro ring resonator ranged from 0.1 to 0.95. The nonlinear refractive index is $n_2 = 2.2 \times 10^{-13}$ m^2/W. In this case, the wave guided loss used is 0.5 dB mm^{-1}. The input soliton pulse is chopped (sliced) into the smaller signals spreading over

the spectrum (i.e. broad wavelength) as shown in Fig. 13(b) and (g), which is shown that the large bandwidth signal is generated within the first ring device. The biggest output amplification is obtained within the nano-waveguides (rings R_3 and R_4) as shown in Figs. 13(d) and (e), whereas the maximum power of 10 W is obtained at the center wavelength of 1.5 μm. The coupling coefficients are given as shown in the figures. The coupling loss is included due to the different core effective areas between micro and nanoring devices, which is given by 0.1 dB.

4. Applications

The application of this proposed work can be categorized into three cases, firstly, we have shown that the multi-wavelength bands can be generated by using a Gaussian pulse propagating within the microring resonator system, which is available for the extended DWDM with the wavelength center at 400–1400 nm, which can be used in the existed public network. Results obtained have shown that the spatial pulses width of 30 nm and the spectrum range of 400 nm can be generated and achieved. Moreover, the problem of signal collision can be solved by using the suitable FSR design [21], while the dispersion

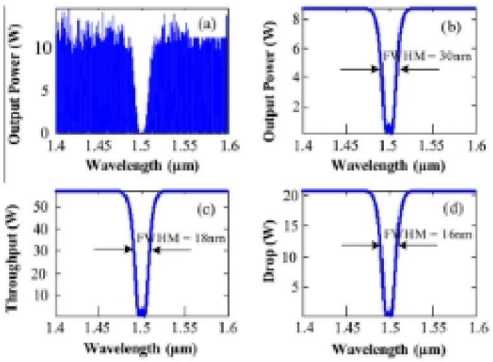

Fig. 11. The dynamic dark soliton (optical tweezers) occurs within add/drop tunable filter, when the bright soliton is input into the add port with the center wavelength λ_0 = 1.5 μm: (a) add/drop signals, (b) dark-bright soliton collision, (c) optical tweezers at throughput port, and (d) optical tweezers at drop port.

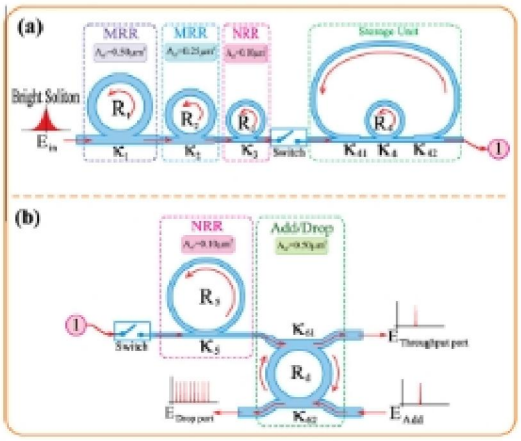

Fig. 12. A broadband generation system: (a) a broadband source generation and a storage unit, (b) a soliton band selector, where R_n, ring radii, κ_n, coupling coefficients, κ_{d1}, κ_{d2}, coupling losses, κ_{s1} and κ_{s2} are the add/drop coupling coefficients.

effect is minimized when the center wavelength at 1.30 μm. Furthermore, the Gaussian pulse output power can be amplified, which can provide the power budget for long distance link. We find that the maximum power of 400 W can be obtained, however, the coupling coefficient of the add/drop filter is the major parameter of the required coupling output power, for instance, the output power of 12 W is obtained as shown in Fig. 6(b), where the parameters are R_d = 5.0 μm, $\kappa_3 = \kappa_4 = 0.9$. This means that the use of wavelength 0.4–1.40 μm (Gaussian pulse) for DWDM via optical communication is plausible, which can be used with the existed public network installation.

Secondly, the dynamic dark soliton control can be configured to be an optical dynamic tool known as an optical tweezers, where more details of optical tweezers can be found in references [23,24]. The optical tweezers behavior is occurred when the bright soliton input is added into the system via add port as shown in Fig. 2, where the parameters of system are used the same as the previous case. The bright soliton is generated with the central wavelength λ_0 = 1.5 μm, when the bright soliton propagating into the add/drop system, the dark-bright soliton collision in add/drop system is seen as shown in Figs. 10(a) and (b). The optical tweezers probe can be trapped/confined atom/light within the well of the probe. The dark soliton valley dept, i.e. potential well is changed when it is modulated by the trapping energy (dark-bright solitons interaction) as shown in Fig. 11. The recovery photon can be obtained by using the dark-bright soliton conversion, which is well analyzed by Sarapat et al. [14], where the trapped photon or molecule can be released or separated from the dark soliton pulse, in practice, in this case the bright soliton is become alive and seen.

Finally, we have shown that a large bandwidth of the optical signals with the specific wavelength can be generated within the micro ring resonator system as shown in Fig. 12. The amplified signals with broad spectrum can be generated, stored and regenerated within the nano-waveguide. The maximum stored power of 10 W is obtained as shown in Fig. 13(d) and (e),

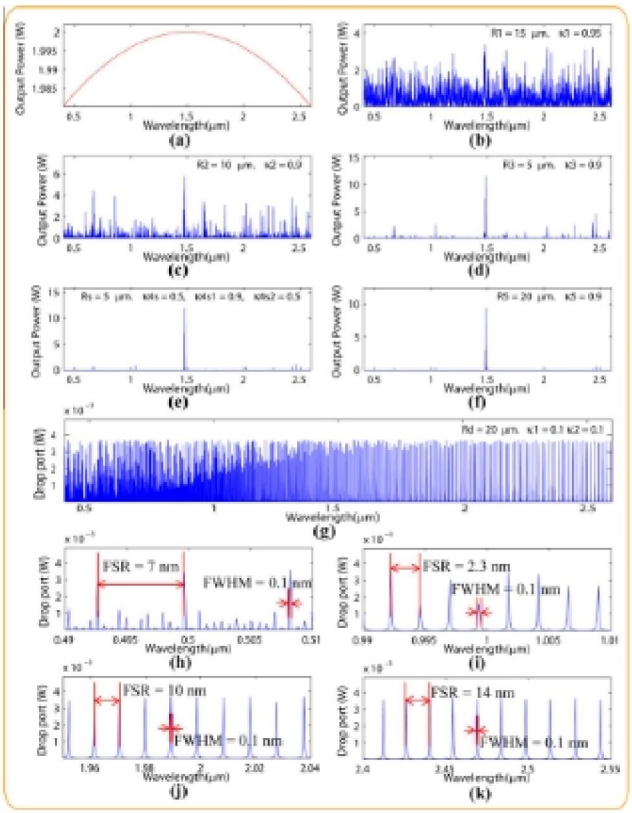

Fig. 13. A soliton band with m, where (a) input soliton, (b) ring R_1 (c) ring R_2, (d) ring R_3, (e) storage ring (R_4), (f) ring R_5, (g) drop port output signals. The output of different soliton bands (center wavelength) are as shown, where (h) 0.51 μm, (i) 0.98 μm (j) 1.99 μm and (k) 2.48 μm.

where the average regenerated optical output power of 4 W is achieved via and a drop port of an add/drop filter as shown in Fig. 13(h)–(k), which is a broad spectra of light cover the large bandwidth as shown in Fig. 13(g). However, to make the system being realistic, the waveguide and connection losses are required to address in the practical device, which may be affected the signal amplification. The storage light pulse within a storage ring (R_s or R_4) is achieved, which has also been reported by Ref. [11]. In applications, the increasing in communication channel and network capacity can be formed by using the different soliton bands (center wavelength) as shown in Fig. 13, where (h) 0.51 μm, (i) 0.98 μm, (j) 1.48 μm and (k) 2.46 μm are the generated center wavelengths of the soliton bands. The selected wavelength center can be performed by using the designed add/drop filter, where the required spectral width (full width at half maximum, FWHM) and free spectrum range (FSR) are obtained, the channel spacing and bandwidth are represented by FSR and FWHM, respectively, for instance, the FSR and FWHM of 2.3 nm and 100 pm are obtained as shown in Fig. 13(i).

5. Conclusion

We have demonstrated that some interesting results can be obtained when the laser pulse is propagated within the nonlinear optical ring resonator, especially, in microring and nanoring resonators, which can be used to perform many applications. For instance, the broad spectrum of a monochromatic source with the reasonable power can be generated and achieved by using a Gaussian pulse, where a dark soliton can be converted to be a bright soliton by using the ring resonator system incorporating the add/drop multiplexer, which can be configured as a dynamic optical tweezers. Moreover, the use of a bright soliton can provide the non-dispersion soliton, where the generation of soliton communication bandwidth with the center wavelength at 1.30 μm is achieved.

References

[1] G.P. Agarwal, Nonlinear Fiber Optics, fourth ed., Academic Press, New York, 2007.
[2] A. Hasegawa (Ed.), Massive, WDM and TDM Soliton Transmission Systems, Kluwer Academic Publishers, 2000.
[3] Yu.A. Simonov, J.A. Tjon, Soliton–soliton interaction in confining models, Phys. Lett. B 85 (1979) 380–384.
[4] J.K. Drohm, L.P. Kok, Yu.A. Simonov, J.A. Tjon, A.I. Veselov, Collision and rotation of solitons in three space–time dimensions, Phys. Lett. B 101 (1981) 204–208.
[5] T. Iizuka, Yu.S. Kivshar, Optical gap solitons in nonresonant quadratic media, Phys. Rev. E 59 (1999) 7148–7151.
[6] A. Biswas, Dispersion-managed solitons in optical fibers, J. Opt. A 4 (1) (2002) 84–97.
[7] R. Kohl, D. Milovic, E. Zerrad, A. Biswas, Soliton perturbation theory for dispersion-managed optical fibers, J. Nonlinear Opt. Phys. Mater. 18 (2) (2009) 227–270.
[8] R. Ganapathy, K. Porsezian, A. Hasegawa, V.N. Serkin, Soliton interaction under soliton dispersion management, IEEE J. Quantum Electron. 44 (2008) 383–390.
[9] N. Pornsuwancharoen, U. Dunmeekaew, P.P. Yupapin, Multi-soliton generation using a micro ring resonator system for DWDM based soliton communication, Microw. Opt. Technol. Lett. 51 (5) (2009) 1374–1377.
[10] P.P. Yupapin, N. Pornsuwanchroen, S. Chaiyasoonthorn, Attosecond pulse generation using nonlinear micro ring resonators, Microw. Opt. Technol. Lett. 50 (12) (2008) 3108–33011.
[11] N. Pornsuwancharoen, P.P. Yupapin, Generalized fast, slow, stop, and store light optically within a nano ring resonator, Microw. Opt. Technol. Lett. 51 (4) (2009) 899–902.
[12] N. Pornsuwancharoen, S. Chaiyasoonthorn, P.P. Yupapin, Fast and slow lights generation using chaotic signals in the nonlinear micro ring resonators for communication security, Opt. Eng. 48 (1) (2009) 50003-1–50005-5.
[13] P.P. Yupapin, N. Pornsuwancharoen, Proposed nonlinear micro ring resonator arrangement for stopping and storing light, IEEE Photon. Technol. Lett. 21 (2009) 404–406.
[14] K. Sarapat, N. Sangwara, K. Srinuanjan, P.P. Yupapin, N. Pornsuwancharoen, Novel dark-bright optical solitons conversion system and power amplification, Opt. Eng. 48 (2009) 045004-1–045004-7.
[15] S. Mitatha, N. Pornsuwancharoen, P.P. Yupapin, A simultaneous short-wave and millimeter-wave generation using a soliton pulse within a nanowaveguide, IEEE Photon. Technol. Lett. 21 (2009) 932–934.
[16] M.E. Heidari, M.K. Moravvej-Farshi, A. Zariffkar, Multichannel wavelength conversion using fourth-order soliton decay, J. Lightwave Technol. 25 (2007) 2571–2578.
[17] A. Charoenmee, N. Pornsuwancharoen, P.P. Yupapin, Trapping a dark soliton pulse within a nano ring resonator, Int. J. Light Electron Opt. (2009), doi:10.1016/j.ijleo.2009.03.015.
[18] D. Deng, Q. Guo, Ince-Gaussian solitons in strongly nonlocal nonlinear media, Opt. Lett. 32 (2007) 3206–3208.
[19] Y. Kokubun, Y. Hatakeyama, M. Ogata, S. Suzuki, N. Zaizen, Fabrication technologies for vertically coupled micro ring resonator with multilevel crossing busline and ultracompact-ring radius, IEEE J. Sel. Top. Quant. Electron. 11 (2005) 4–10.
[20] Y. Su, F. Liu, Q. Li, System performance of slow-light buffering, and storage in silicon nano-waveguide, Proc. SPIE 6783 (2007) 67832P.
[21] P.P. Yupapin, P. Saeung, C. Li, Characteristics of complementary ring-resonator add/drop filters modeling by using graphical approach, Opt. Commun. 272 (2007) 81–86.
[22] P.P. Yupapin, W. Suwancharoen, Chaotic signal generation and cancellation using a micro ring resonator incorporating an optical add/drop multiplexer, Opt. Commun. 280 (2) (2007) 343–350.
[23] L. Yuan, Z. Liu, J. Yang, C. Guan, Twin-core fiber optical tweezers, Opt. Exp. 16 (2008) 4559–4566.
[24] N. Malagninoa, G. Pescea, A. Sassoa, E. Arimondo, Measurements of trapping efficiency and stiffness in optical tweezers, Opt. Commun. 214 (2007) 15–24.

Optik 122 (2011) 306–309

Contents lists available at ScienceDirect

Optik

journal homepage: www.elsevier.de/ijleo

Multiphotons trapping instability using fiber Bragg's grating potential perturbation for multiquantum bits encoding

B. Vanishkorn, K. Srinuanjan, P.P. Yupapin*

Advanced Research Center for Photonics, Faculty of Science, King Mongkut's Institute of Technology Ladkrabang, Bangkok 10520, Thailand

ARTICLE INFO

Article history:
Received 18 June 2009
Accepted 2 March 2010

Keywords:
Multiphotons
Quantum bits encoding
Grating potential model
Potential perturbation

ABSTRACT

We propose an interesting result of the trapped multiphotons distribution within a fiber Bragg's grating. The multitrapped photons are confined by the potential well, where the motion of photons in a fiber Bragg's grating is affected by the external perturbations, which they are defined as a series of nonlinear parametric in terms of potential energy. This investigation is modeled by using the nonlinear coupled mode equations and under Bragg's resonance condition, where the initial frequency of the light, ω_0 is the same value as the Bragg's frequency, ω_g. Results obtained have shown that the higher perturbation series represents the potential well is much differed from the equilibrium situation. In applications, the external perturbations on the fiber grating can cause the trapped photons instability, which introduces the escaped photons from the potential well being detected and observed. The potential of applications for quantum encoding device can be performed, which is analyzed and discussed in details.

1. Introduction

Quantum information has been the interesting technology of the communication for the secret information area today. Because of the additional advantage of the secret key information obtained by the cryptographic technique is the significant application improvement. Several research works using quantum information have been reported [1,2], where they have shown that the use of quantum communication and network could be implemented in the different media [3,4]. However, the searching of new devices for quantum technology remains, where one of them is the common device called a fiber Bragg's grating (FBG), which is useful in many applications. FBG in optical fibers have been demonstrated in a wide range of applications such as for sensors, dispersion compensators, optical fiber filter and all optical switching and routing. Therefore, numerous research works are directed towards investigation of pulse propagation in FBGs. Periodically structured optical media have been in the clarity of research activity for many years, due to versatile technologies applications in the fields of telecommunications and sensor system [5], and also as a subject of fundamental studies [6]. At the early stage of the work in this area, the pioneering contribution by Winful et al. [7] laid the groundwork for extensive theoretical activities exploring nonlinear pulse propagating in one-dimensional periodic structure known as fiber Bragg's gratings. They have considered the role of the Kerr nonlinearity in the light transmission through the FBGs. Bragg's gratings in optical fibers are excellent devices for studying nonlinear phenomena particularly based on the Kerr nonlinearity [8]. These structures are based on the periodic modulation of the local periodic modulation of the local refractive index in the axial direction. A characteristic feature of FBGs is a stopband, alias photonic bandgap, in their linear-propagation spectrum. The bandgap is induced by the resonant coupling between the forward- and backward-propagating waves due to the Bragg's resonance [9]. The stationary properties of one-dimensional Bragg's gratings were first analyzed by Winful et al. [10]. Many research papers on the existence of soliton in FBGs have been reported [11–15], where they have derived the formation of bright and gap soliton solution for nonlinear coupled mode equation, which governs the pulse propagation in FBG. In this paper we further describe the effect of α and γ to obtain the optimized point of the potential well. The motion of a particle moving in FBG represents the pulse propagation in the grating structure of fiber optics exhibiting the existence of optical soliton. In order to describe the photon motion, the function of potential energy is depicted. Photon can be trapped by some parameters of potential energy such as α and γ. The other parameter, theta, θ is introduced to describe any disturbance effect of moving particle having specific energy. In applications, the use of FBG for various applications, for instance, entangle photon source, quantum sensor and quantum encoding can be configured when the external perturbation is applied on the grating, which may be realized in the near future.

* Corresponding author. Fax: +66 2 3264334.
E-mail address: kypreech@kmitl.ac.th (P.P. Yupapin).

0030-4026/$ – see front matter © 2010 Elsevier GmbH. All rights reserved.
doi:10.1016/j.ijleo.2010.03.013

2. Multiphotons potential energy distribution

Wave propagation in FBG is analyzed by solving Maxwell's equation with appropriate boundary conditions. In the presence of Kerr nonlinearity, using the coupled-mode theory, the nonlinear coupled mode equation is defined under the absence of material and waveguide dispersive effects. The dispersion arising from the periodic structure dominates near Bragg's resonance conditions and it is valid only for wavelengths near to the Bragg's wavelength. By substituting the stationary solution to the coupled mode equation and by assuming $E_{\pm}(z,t) = e_{\pm}(z)e^{-i\delta ct/n}$, we obtain Eq. (1) [5]:

$$i\frac{de_f}{dz} + \hat{\delta}e_f + \kappa e_b + \left(\Gamma_S\left|e_f\right|^2 + 2\Gamma_X\left|e_b\right|^2\right)e_f = 0$$
and
$$-i\frac{de_b}{dz} + \hat{\delta}e_b + \kappa e_f + \left(\Gamma_S\left|e_b\right|^2 + 2\Gamma_X\left|e_f\right|^2\right)e_b = 0 \quad (1)$$

Eq. (1) represents the time-independent light transmission through the gratings structure where e_f and e_b are the forward- and backward-propagating modes. In order to explain the formation of Bragg's soliton, we consider the Stokes parameter [15], since it will provide useful information about the total energy and energy difference between the forward-and backward-ropagating modes, which is given by the relation as

$$A_0 = \left|e_f\right|^2 + \left|e_b\right|^2,$$
$$A_1 = e_f e_b^* + e_f^* e_b,$$
$$A_2 = i\left(e_f e_b^* - e_f^* e_b\right), \quad (2)$$
$$A_3 = \left|e_f\right|^2 - \left|e_b\right|^2$$

with the constraint $A_0^2 = A_1^2 + A_2^2 + A_3^2$. In the FBG theory, the nonlinear coupled mode (NLCM) equation requires that the total power $P_0 = A_3 = \left|e_f\right|^2 - \left|e_b\right|^2$ inside the grating is constant along the grating structures. Rewriting the NLCM equations in terms of Stokes parameter gives

$$\frac{dA_0}{dz} = -2\kappa A_2, \quad \frac{dA_1}{dz} = 2\hat{\delta}A_2 + 3\Gamma A_0 A_2,$$
$$\frac{dA_2}{dz} = -2\hat{\delta}A_1 - 2\kappa A_0 - 3\Gamma A_0 A_1, \quad \frac{dA_3}{dz} = 0 \quad (3)$$

In Eq. (3), we drop the distinction between the Self-Phase Modulation and cross effect modulation effects and hence it becomes $3\Gamma = 2\Gamma_x + \Gamma_z$. It can be clearly shown that the total power, $P_0 (= A_3)$ inside the grating is found to be constant or conserved along the grating structure [16]. In the construction of the anharmonic oscillator type equation, it is necessary to use the conserved quantity, and it is obtained in the form $\hat{\delta}A_0 + \frac{3}{4}\Gamma A_0^2 + \kappa A_1 = C$, where C is the constant of integration and $\hat{\delta}$ is the detuning parameter. Using Eq. (3), we obtain

$$\frac{d^2A_0}{dz^2} - \alpha A_0 + \beta A_0^2 + \gamma A_0^3 = 4\hat{\delta}C \quad (4)$$

where $\alpha = 2\left[2\hat{\delta}^2 - 2\kappa^2 - 3\Gamma C\right]$, $\beta = 9\Gamma\hat{\delta}$ and $\gamma = \frac{9}{4}\Gamma^2$. Eq. (4) contains all the physical parameter of the NLCM equation.

In order to describe the motion of a particle moving with the classic anharmonic potential, where the external disturbance is involved then we have the solution as

$$V(A_0) = -\alpha\frac{A_0^2}{2} + \beta\frac{A_0^3}{3} + \gamma\frac{A_0^4}{4} \quad (5)$$

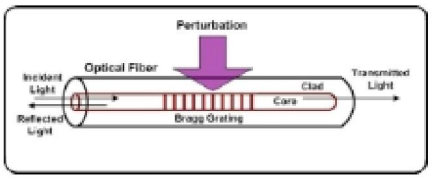

Fig. 1. A schematic of light propagating within a fiber Bragg's grating with perturbation.

It represents the potential energy distribution in the fiber Bragg's grating structures. The generated photons under stability condition are confined within the potential well, which there is no output light obtained and observed in this situation. However, the perturbation on the grating will break the stability condition, where the photons can be escaped from the potential well and observed.

3. Multiphotons trapping instability

Consider Eq. (2) having a set of constraints which is introduced by $\phi_{(e)} = \sum_{m=0}^{\infty} A_0^n$ as a function of perturbation factor then

$$\frac{d^2A_0}{dz^2} = \phi_e^{\sigma}| \quad (6)$$

If Eq. (4) is accumulated using external perturbation then

$$\phi^{\sigma}| + \sum_{\substack{n=0 \\ m=1}}^{\infty} C_m A_0{}^n = \psi$$

where ψ is a function of $f(\delta, C, C_m)$ and $C_m = [\alpha, \beta, \gamma, \ldots]$. The value of $m = 2n$ for $n = 1, 2, 3, \ldots$, $m = 2n + 1$ for $n = 0, 1, 2, \ldots$. C is constant and $C = (C_1, C_2, C_3, \ldots, C_m)$. The value of C is linear to A_0 but not to V. Eq. (5) can then be modified by

$$V(A_0) = \sum_{\substack{m=1 \\ n=0}}^{\infty} C_m A_0^n \quad (7)$$

Eq. (7) represents the complete potential energy distribution in the fiber Bragg's grating structure. We believe at this juncture, the potential function is modified from Conti and Trillo [17]. Using well-known Duffing oscillator type equation, analogically it is written as

$$\phi_e^{\sigma} + \sum_{\substack{m=1 \\ n=0}}^{\infty} C_m A_0^n = 0 \quad (8)$$

For multiperturbation of nonlinear parametric, two major shapes will be simplified in series term.

Fig. 1 depicts the fiber length when the external perturbation is applied on the fiber grating. It is induced the change in potential well parameters, and the photons trapping instability is occurred. Fig. 2 depicts the motion of photon in potential well changes when few nonlinear parameters are taken into account as shown in Eq. (5). There are theoretically some comments in this figure. Photon is trapped by α parameter which is depicted by legend V. When α is too large, the potential well produces A_0 and a wider double well. The parameter γ range is shown by X legend. When γ is large, the potential well produces an increase in A_0. When light is launched

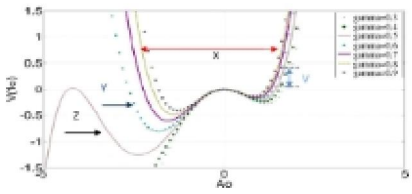

Fig. 2. The motion of photon in potential well for $\alpha = 0.5$, $\beta = 0.3$, $\theta = 0.09$ and γ is varies from 0.3 to 0.9.

into the FBG, the trapped photons (particles) are generated and confined within the grating. It shows that double well potential well is not symmetric and potential energy will decrease within the region at legend *Y*. The other effect is the perturbation of potential energy by legend *Z* where photon cannot be trapped symmetrically. It will tend to equilibrate but it is not stable where it will lead to losses.

The stationary solutions of Eq. (4) are applied neither for bright nor dark soliton solution since the dominant parameters in contributing A_0 is unknown. However, from Eq. (4) we have

$$A_0 = A_0(C_m, z) \tag{9}$$

Under these conditions, the frequencies with photonic band gap keep forming an envelope after the exact balancing at grating-induced dispersion with nonlinearity. It either decays or increases with the forward and backward waves being transferred by the Bragg's reflection process. The total energy of the system, potential energy function is equal to zero having multiperturbation which is $-1 < A_0 < 1$ and if $V \to \infty$, $A_0 = 2$.

In term of parametric function, we can describe it as follows. The change in α will affect the dip of the potential well. When α is approximately too small, the shape of the potential well will turn into a single potential well. The occurrence of β effect in the motion of photon will give effect to the negative region for $A_0 < 0$. The effect of γ shows that the width of potential well will decrease if the value of γ is increased. Therefore, if the value of γ is increased, we can assume that the photon is localized and trapped. Another nonlinear factor (i.e. θ) can change the shape of potential well rapidly. When the existence of θ is included, the shape of potential well becomes chaotic. The photon does not only move in certain region known as potential well but also can be termed as free moving particles. Fig. 3 explains the extrapolation of the graph if more factors of perturbation added into Eq. (7). The addition of parametric factors by the higher odd number in Fig. 3(b) leads the photon to be untrapped, where the higher even number in Fig. 3(a) allows the photon to move in a well. It is clearly shown in the graphs that as $n \gg \infty$, the value of $|A_0|$ remains constant in the range of $-2 < A_0 < 2$. However, when the value of $V_{(0)}$ is equal to zero, there are many possibilities of A_0, meaning the exact value of intentsity, A_0 to trap the photon is difficult to determine in this condition. When the parametric factor is considered is too large then we may conclude that the photon is in indifferent state part of the equlibrium.

4. Multiquantum bits encoding

Let us consider that the case when the multiphotons is perturbed and input into the quantum processor unit as shown in Fig. 4. Generally, there are pairs of possible polarization entangled photons forming within the ring device, which are represented by the four polarization orientation angles as $|0^\circ, 90^\circ|$, $|135^\circ$ and $180^\circ|$. These can be formed by using the optical component called the polarization rotatable device and a polarizing beam splitter (PBS). In this

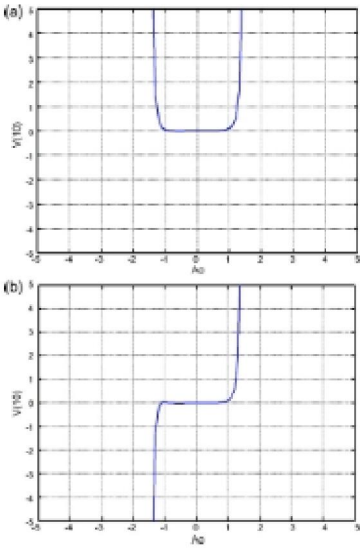

Fig. 3. Illustration of potential well when the disturbance factor that affect the shape of the potential well of the motion of photon, where (a) stability and (b) instability potential wells.

concept, we assume that the polarized photon can be performed by using the proposed arrangement, where each pair of the transmitted qubits can be randomly formed the entangled photon pairs. To begin this concept, we introduce the technique that can be used to create the entangled photon pair (qubits) as shown in Fig. 4, a polarization coupler that separates the basic vertical and horizontal polarization states corresponds to an optical switch between the short and the long pulses. We assume those horizontally polarized pulses with a temporal separation of Δt. The coherence time of the consecutive pulses is larger than Δt. Then the following state is created by Eq. (10) [4]:

$$|\Phi\rangle_p = |1, H\rangle_s |1, H\rangle_l + |2, H\rangle_s |2, H\rangle_l \tag{10}$$

In the expression $|k, H\rangle$, k is the number of time slots (1 or 2), where denotes the state of polarization [horizontal $|H\rangle$ or vertical

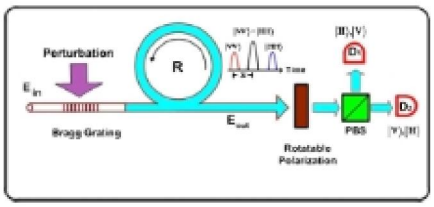

Fig. 4. A schematic of an entangled photon pair manipulation within a ring resonator connecting to the FBG. The Bell's state is propagating to a rotatable polarizer and then is split by a beam splitter (PBS) flying to detector D_1 and D_2.

$|V\rangle$], and the subscript identifies whether the state is the signal (s) or the idler (i) state. In Eq. (10), for simplicity, we have omitted an amplitude term that is common to all product states. We employ the same simplification in subsequent equations in this paper. This two-photon state with $|H\rangle$ polarization shown by Eq. (10) is input into the orthogonal polarization-delay circuit shown schematically. The delay circuit consists of a coupler and the difference between the round-trip times of the micro ring resonator, which is equal to (t. The micro ring is tilted by changing the round trip of the ring is converted into $|V\rangle$ at the delay circuit output. That is the delay circuits convert $|k, H\rangle$ to be

$$r|k, H\rangle_{it_2} \exp(i\phi)|k+1, V\rangle_{,} rt_2 \exp(i_2\phi)|k+2, H\rangle_{,} r_2 t_2 \exp(i_3\phi)|k+3, V$$

where t and r is the amplitude transmittances to cross and bar ports in a coupler. Then Eq. (10) is converted into the polarized state by the delay circuit as

$$\begin{aligned}
|\Phi\rangle &= [|1,H\rangle_s + \exp(i\phi_s)|2,V\rangle_s] \times [|1,H\rangle_i + \exp(i\phi_i)|2,V\rangle_i] \\
&\quad + [|2,H\rangle_s + \exp(i\phi_s)|3,V\rangle_s] \times [|2,H\rangle_i + \exp(i\phi_s)|2,V\rangle_i] \\
&= |1,H\rangle_s|1,H\rangle_i + \exp(i\phi_i)|1,H\rangle_s|2,V\rangle_i + \exp(i\phi_s)|2,V\rangle_s|1,H\rangle_i \\
&\quad + \exp[i(\phi_s+\phi_i)]|2,V\rangle_s|2,V\rangle_i + |2,H\rangle_s|2,H\rangle_i \\
&\quad + \exp(i\phi_s)|2,H\rangle_s|3,V\rangle_i + \exp(i\phi_s)|3,V\rangle_s|2,H\rangle_i \\
&\quad + \exp[i(\phi_s+\phi_i)]|3,V\rangle_s|3,V\rangle_i
\end{aligned} \tag{11}$$

By the coincidence counts in the second time slot, we can extract the fourth and fifth terms. As a result, we can obtain the following polarization entangled state as

$$|\Phi\rangle = |2,H\rangle_s|2,H\rangle_i + \exp[i(\phi_s+\phi_i)]|2,V\rangle_s|2,V\rangle_i \tag{12}$$

We assume that the response time of the Kerr effect is much less than the cavity round-trip time. Because of the Kerr nonlinearity of the optical device, the strong pulses acquire an intensity dependent phase shift during propagation. The interference of light pulses at a coupler introduces the output beam, which is entangled. Due to the polarization states of light pulses are changed and converted while circulating in the delay circuit, where the polarization entangled photon pairs can be generated. The entangled photons of the nonlinear ring resonator are separated to be the signal and idler photon probability. The polarization angle adjustment device is applied to investigate the orientation and optical output intensity, this concept is well described by the published work [14].

5. Conclusion

We successfully modified and developed the potential energy distribution of photon by setting the disturbance of multiperturbation potential energy in a fiber Bragg's grating. It is found that the potential well under Bragg's resonance condition is not symmetrical and conserved. The higher perturbation series representing the potential well is much differed from the equilibrium in both odd and even nonlinear parametric factor of n. In applications, the multiphotons trapping within the potential well are introduced by the propagating soliton in the FBG, which they are localized and stable within the Fabry–Perot barrier. However, they can be escaped from the well and seen after the perturbation. By using the suitable photon squeezing conditions incorporating the quantum signal processor, where the use of the proposed design for multiquantum bits generation is plausible.

References

[1] M. Raginsky, P. Kumar, Generation and manipulation of squeezed states of light in optical networks for quantum communication and computation, J. Opt. B: Quantum Semiclass. Opt. 3 (2001) L1–L4.
[2] M. Lassen, M. Sabuncu, P. Buchhave, U.L. Andersen, Generation of polarization squeezing with periodically poled KTP at 1064 nm, Opt. Exp. 15 (8) (2007) 5077–5082.
[3] P.P. Yupapin, P. Phiphithirankarn, S. Suchat, A quantum CODEC design via an optical add/drop multiplexer in a fiber optic network, Far East. J. Electron. Commun. 1 (3) (2007) 259–267.
[4] S. Suchat, W. Khannam, P.P. Yupapin, Quantum key distribution via an optical wireless communication link for telephone network, Opt. Eng. Lett. 46 (10) (2007) 100502.
[5] R. Kashyap, Fiber Bragg Gratings, Academic Press, San Diego, 1999.
[6] B.A. Malomed, Soliton Management in Periodic Systems, Springer, New York, 2006.
[7] H.G. Winful, J.H. Marburger, E. Garmire, Theory of bistability in nonlinear distributed feedback structures, Appl. Phys. Lett. 35 (1979) 379–381.
[8] Y.S. Kivshar, G.P. Agrawal, Optical Soliton: From Fibers to Photonics Crystal, Academic Press, USA, 2003.
[9] K.W. Chow, I.M. Merhasin, B.A. Malomed, K. Nakkeeran, K. Senthilnathan, P.K.A. Wai, Periodic waves in fiber Bragg gratings, Phys. Rev. E. 77 (2008) 026602.
[10] K. Senthilnathan, K. Porsezian, Symmetry-breaking instability in gap soliton, Opt. Commun. 227 (2003) 295–299.
[11] K. Porsezian, K. Senthilnathan, Guided Wave Optical Components and Devices: Basics, Technology and Applications, Academic Press, USA, 2006, pp. 251–279.
[12] W. Chen, D.L. Mills, Gap solitons and the nonlinear optical response of supper lattices, Phys. Rev. Lett. 58 (1987) 160–163.
[13] D.L. Mill, S.E. Trullinger, Gap solitons in nonlinear periodic structures, Phys. Rev. B 36 (1987) 947–952.
[14] J.E. Sipe, H.G. Winful, Nonlinear Schrödinger solitons in a periodic structure, Opt. Lett. 13 (1988) 132–134.
[15] D.N. Christodoulides, R.I. Joseph, Slow Bragg solitons in nonlinear periodic structures, Phys. Rev. Lett. 62 (1989) 1746–1748.
[16] A.B. Aceves, S. Wabnitz, Self-induced transparency solitons in nonlinear refractive periodic media, Phys. Lett. A 141 (1989) 37–39.
[17] C. Conti, S. Trillo, Bifurcation of gap solitons through catastrophe theory, Phys. Rev. E 64 (2001) 036617.

Author Biography

Name	Mr. Buddhaporn Vanishkorn
Date of Birth	20 December 1979
Address	369/68, Naiklongbangplakod, Prasamutjadee, Samutprakarn 10290.
Education	1998 Bachelor of Science in Applied Mathematics GPA 2.42 King Mongkut's University of Technology Thonburi, Bangkok Thailand.
	2002 Master of Science in Applied Mathematics GPA 3.26 King Mongkut's University of Technology Thonburi, Bangkok Thailand.
Scholarship	2009-2012 scholarship from king mongkut's institute of technology ladkrabang.

Academic Publications

1. Yupapin, P.P., Vanishkorn, B. 2011. **"Mathematical simulation of light pulse propagating within a microring resonator system and applications."** Applied Mathematical Modelling. 35 : 1729-1738.
2. Vanishkorn, B. Srinuanjan, K. Yupapin, P.P. 2011. **"Multiphotons trapping instability using fiber Bragg's grating potential perturbation for multiquantum bits encoding."** Optik. 122 : 506-509.